Anatomical organization of the brain of a diurnal and a nocturnal dung beetle

Esa-Ville Immonen[1], Marie Dacke[1], Stanley Heinze[1], and Basil el Jundi[1]

[1]: Lund Vision Group, Department of Biology, Lund University, 22362 Lund, Sweden

Abbreviated title: Neuroarchitecture of the dung beetle brain

Associate editor: Ian A. Meinertzhagen

Keywords: *Scarabaeus*; sensory ecology; optic lobe; central complex; mushroom body; antennal lobe; RRID: SCR_002285; RRID: SCR_007353; RRID: AB_2315426; RRID: AB_572263

Corresponding author: Esa-Ville Immonen, Lund Vision Group, Department of Biology, Lund University, Sölvegatan 35, 22362, Lund, Sweden; phone: +46 46 222 9578; e-mail: esa-ville.immonen@biol.lu.se

ABSTRACT

To avoid the fierce competition for food, South African ball-rolling dung beetles carve a piece of dung off a dung-pile, shape it into a ball and roll it away along a straight line path. For this unidirectional exit from the busy dung pile, at night and day, the beetles use a wide repertoire of celestial compass cues. This robust and relatively easily measurable orientation behavior has made ball-rolling dung beetles an attractive model organism for the study of the neuroethology behind insect orientation and sensory ecology. Although there is already some knowledge emerging concerning how celestial cues are processed in the dung beetle brain, little is known about its general neural layout. Mapping the neuropils of the dung beetle brain is thus a prerequisite to understand the neuronal network that underlies celestial compass orientation. Here, we describe and compare the brains of a day-active and a night-active dung beetle species based on immunostainings against synapsin and serotonin. We also provide 3D reconstructions for all brain areas and many of the fiber bundles in the brain of the day-active dung beetle. Comparison of neuropil structures between the two dung beetle species revealed differences that reflect adaptations to different light conditions. Altogether, our results provide a reference framework for future studies on the neuroethology of insects in general and dung beetles in particular.

INTRODUCTION

Recent studies on insect navigation and the neural principles behind it (for example, Homberg et al., 2011; el Jundi et al., 2014; Webb and Wystrach, 2016) provide us with novel insights into one of the fundamental question in neuroscience: How does a brain control behavior? With a robust orientation behavior and a brain that is often physiologically accessible, insects are ideal organisms to explore this question further. Among the prime examples of such insects are South African ball-rolling dung beetles, active during the day (*Scarabaeus lamarcki*) as well as during the night (*Scarabaeus satyrus*). Due to high competition for food at a dung pile, these dung feeding beetles carve a wet piece from the pile, shape it into a ball and roll it away along a straight path, using celestial cues as their only visual source of reference (Byrne et al., 2003; Dacke et al., 2003a, 2004, 2013a; b, 2014, el Jundi et al., 2014b, 2015a; b). Recently it has been shown that dung beetles maintain their exit direction by performing a dance (Baird et al., 2012), during which they take a snapshot of the sky to use as a template for their compass while rolling (el Jundi et al., 2016). Based on a combination of behavioral experiments and single neuron electrophysiology, the hierarchy of the main celestial signals (polarized light and celestial body) has recently been established in a set of neurons in the dung beetle's central brain (el Jundi et al., 2015b).

The region where these "compass" neurons in the dung beetle brain lie is known as the central complex, a group of modular neuropils that are highly conserved among insects (Homberg, 2008). The central complex is involved in a variety of behaviors including visual information processing during flight (Weir et al., 2014; Weir and Dickinson, 2015), obtaining a sense of direction by combining self-motion cues with visual landmarks (Seelig and Jayaraman, 2015; Varga and Ritzmann, 2016), initiation and control of locomotion (Bender et al., 2010; Guo and Ritzmann, 2013; Martin et al., 2015), and formation of spatial memory (Ofstad et al., 2011). Experiments in migratory species, such as locusts and monarch butterflies, suggest that the central complex acts as an internal compass (Heinze and Homberg, 2007; Heinze and Reppert, 2011; Homberg et al., 2011; el Jundi et al., 2014a) to help these animals

find their travel destination. Before reaching the central-complex network, the celestial cues are pre-processed in different brain regions such as the optic lobes, the anterior optic tubercle and the lateral complex (Homberg et al., 2011; Heinze et al., 2013; el Jundi et al., 2014a).

Like many other insects, dung beetles also strongly rely on olfactory cues for locating the preferred type of food (dung), as well as mates for copulation (Dormont et al., 2010; Tride and Burger, 2011; Burger, 2014). The related compounds are detected by antennal olfactory receptor neurons that project to the the first order olfactory neuropils; the antennal lobes (reviewed in, e.g., Hansson and Stensmyr, 2011). From here, information is typically sent to higher order centers, including the lateral horns and the mushroom bodies. The latter are considered to be the memory centers of the insect brain, and thus, have been studied extensively (Heisenberg et al., 1985; Heisenberg, 2003; Menzel, 2014; Cohn et al., 2015; Hige et al., 2015; Farris, 2016; Webb and Wystrach, 2016). Recent studies in *Drosophila* have also shown that the mushroom-body output neurons encode the behavioral valence, causing bias to behavioral executions rather than encoding the identity of a given odor (Aso et al., 2014a; b).

Brain regions such as the optic lobes, the antennal lobes, the mushroom bodies and the central complex have often been the subject of intra- and inter-specific comparative neuroanatomical studies with an aim to relate brain polymorphism to behavioral differences. One example of intra-species polymorphism is the sexual dimorphism of the olfactory system in moths (Rospars and Hildebrand, 2000; Schachtner et al., 2005). Inter-species comparison between two closely related moths indicates that the preference for visual cues in the diurnal species is reflected anatomically by a larger brain area dedicated to visual processing, compared to the nocturnal species, in which the olfactory processing neuropils are more prominent (Stöckl et al., 2016a). Recently, it has also been demonstrated that the processing of sky-compass information differs physiologically between day-active (encodes the sun over polarized light) and night-active (encodes polarized light over the moon) dung beetle species (el Jundi et al., 2015b). However, it is still unknown how these different lifestyles affect the neuroarchitecture of the brain at different processing stages.

In addition to the well-defined brain areas, the insect cerebrum consists of regions that exhibit less defined boundaries. These contiguous neuropil regions are linked to the more well-defined ones within the cerebrum, but have gained little attention, even though they comprise a significant proportion of the whole brain (Homberg et al., 1988; Chiang et al., 2011; Jenett et al., 2012; Phillips-Portillo and Strausfeld, 2012; Tanaka et al., 2012b; Ian et al., 2016a). Thus, obtaining a full picture of the neural network underlying a certain behavior requires investigations of the whole brain, including neuropils of the cerebrum with less distinct borders. So far, 3D neuropil maps of such central adjoining neuropils exist for three species, the monarch butterfly *Danaus plexippus* (Heinze and Reppert, 2012), the ant *Cardiocondyla obscurior* (Bressan et al., 2015), and the fruit fly *Drosophila melanogaster* (Ito et al., 2014). The latter study has introduced a nomenclature for defining and naming all neuropils and fibers tracts in the insect brain and provides the basis for uniformly defining the same brain areas in different insects (Ito et al., 2014).

Here, we provide a comprehensive neuropil atlas for two closely related South African ball-rolling dung beetles, the diurnal *Scarabaeus lamarcki* and the nocturnal *Scarabaeus satyrus*. To obtain this atlas, the dung beetle brains were immunohistochemically labeled using antibodies targeting the presynaptic marker protein synapsin and the neurotransmitter serotonin. With this method, we were able to label and reconstruct overall 32 paired and unpaired synapse-rich neuropils, including their substructures, and 21 fiber bundles, covering the whole central brain and the optic lobes. Our work adds to the body of only a few studies (Heinze and Reppert, 2012; Ito et al., 2014; Bressan et al., 2015) where central adjoining neuropils surrounding the central complex are described. The data further demonstrate important implications regarding sensory ecological differences between the studied dung

beetle species (diurnal and nocturnal), and provide a detailed framework for the study of single neuron connectivity between different brain regions.

MATERIALS AND METHODS

Animals

Adult diurnal (*Scarabaeus lamarcki*) and nocturnal (*Scarabaeus satyrus*) dung beetles (family: *Scarabaeidae*; order: *Coleoptera*) were collected in the game reserve "Stonehenge" in South Africa (24.32°E, 26.39°S) and kept in a room at 26°C temperature (12/12 hours day/light cycle) in large sand-filled plastic containers at Lund University, Lund, Sweden. The beetles were fed with cow dung collected from a local farm.

Antibodies

Synapsins are a family of proteins expressed in presynaptic terminals where they are thought to be involved in vesicle trafficking, and thus, in regulating neurotransmitter release. The expression of synapsin among invertebrates appears to be highly conserved (Klagges et al., 1996; Fabian-Fine et al., 1999; Harzsch et al., 1999; Montgomery and Ott, 2015), making it a useful target for comparative studies on insect brain anatomy. To label neuropil structures in the dung beetle brain, a monoclonal anti-synapsin antibody (see Table 1) raised in mice against fusion proteins made of glutathione S-transferase and parts of the *Drosophila* Synapsin (SYNORF1, Klagges et al., 1996) was used (for successful labeling in other species see e.g. Brandt et al., 2005; Kurylas et al., 2008; el Jundi et al., 2009; Dreyer et al., 2010; Heinze and Reppert, 2012; Bressan et al., 2015). The specificity of this antibody has been verified in *Drosophila* (Klagges et al., 1996; Godenschwege et al., 2004). For immunofluorescence detection of anti-synapsin we used Cy5-conjugated goat anti-mouse (GAM-Cy5) secondary antibody (Jackson ImmunoResearch, West Grove, PA, USA; Cat #: 115-175-146).

To stain serotonin-immunoreactive regions in the dung beetle brain we used a polyclonal serotonin antibody (anti-5-HT; see Table 1) raised in rabbits against serotonin (5-HT) coupled to bovine serum albumin (BSA). To test for specificity of this antibody, we performed a preadsorption of anti-5-HT solution (1:10,000 dilution in 0.01 M phosphate buffered saline (PBS) with 0.25% Triton-X 100 (PBT) supplemented with 1% normal goat serum (NGS)) at four different concentrations (0 µg/ml, 0.2 µg/ml, 2 µg/ml and 20 µg/ml) of 5-HT-BSA conjugate (Immunostar, catalog number 20081) for 20 hours at 4°C before incubation on thin sections (40 µm) from two *S. lamarcki* brains. The sections incubated with the solution lacking 5-HT-BSA showed clear anti-5-HT staining, while the staining was very weak with concentrations of 0.2 µg/ml and 2 µg/ml 5-HT-BSA conjugate, and disappeared completely at 20 µg/ml. As a secondary antibody, we used a goat anti-rabbit-Alexa Fluor® 546 conjugate (GAR-Alexa546; Invitrogen Carlsbad, CA, USA lot number: 435414).

Immunocytochemistry

Animals were dissected during their active period, i.e. subjective day and night for the diurnal and nocturnal species, respectively. The abdomen right behind the thorax and the legs were cut off. The remaining body (head capsule and thorax) was then mounted on a piece of wax inside a dish filled with HEPES (2-[4-(2-hydroxyethyl)piperazin-1-yl]ethanesulfonic acid)-buffered saline (HBS; 150 mM NaCl, 5 mM KCl, 5 mM $CaCl_2$, 25 mM sucrose, 10 mM HEPES). The dorsal part of the head capsule was cut out with a razor blade, followed by removal of tissue and trachea around the brain. The brain was removed within 20-30 minutes and transferred into fixative solution.

For wholemounts, we followed a standard protocol for antibody stainings used in large insect brains (Ott, 2008; Stöckl and Heinze, 2015). The brains were first fixated for about two hours at room temperature (20°C) before fixation at 4°C for ~20 hours using zinc-formaldehyde fixative (ZnFA; 18.4 mM $ZnCl_2$, 135 mM NaCl, 35 mM sucrose, 1% paraformaldehyde (PFA)), which facilitates the penetration of antibodies into deeper brain areas (Ott, 2008). After fixation, the brains were washed with HBS for 8 x 20 min at room temperature on a shaker. To facilitate antibody permeation the brains were next treated with a mixture of dimethyl sulfoxide (DMSO) and methanol (80:20 ratio) for 55 minutes followed by 3 x 10 minutes washing in 0.1 M Tris-buffer. They were preincubated overnight at 4°C with 5% normal goat serum (NGS) in phosphate buffered saline (PBS) containing 0.3% Triton X (PBT), followed by five days incubation in the primary antibody solution (1:50 anti-synapsin, 1:10,000 anti-5-HT, 1% NGS in PBT). After washing in PBT (8 x 20 minutes) the brains were incubated for three days in the secondary antibody solution (1:300 GAM-Cy5, 1:600 GAR-Alexa546, 1% NGS in PBT). Subsequently, they were washed for 6 x 20 minutes in PBT and 2 x 20 minutes in PBS before dehydration through an ascending ethanol series (50%, 70%, 90%, 96%, 100%, 15 minutes each). The brains were cleared for 15 minutes in 1:1 ethanol-methyl salicylate followed by methyl salicylate for 35 minutes before they were mounted in Permount (Fisher Scientific, Pittsburg, PA) between two glass coverslips with spacer rings.

For brain sections, we fixated the brain with either 4% formalin in PBS (thick sections; 130 µm) or Zamboni's fixative (4% PFA, 7.5% picric acid in 0.01 M phosphate buffer, pH = 7.4; thin sections, 40 µm). The brains were subsequently washed (2 x 10 minutes) in PBS before embedding in albumin-gelatin (4.8% gelatin and 12% ovalbumin in distilled H_20). After fixation in 4% formalin in PBS (for 40 minutes at room temperature, and then overnight at 4°C) the brains were sectioned using a vibratome (Leica VT1200, Wetzlar, Germany) and washed in PBS for 3 x 10 minutes before incubation in 5% NGS in PBT overnight. Next, the sections were incubated in the same primary antibody solutions as the wholemount samples (see above) for either five days at 4°C (thick sections, 130 µm) or for one day at room temperature (thin sections, 40 µm). All sections were then washed in PBT (8 x 10 minutes) before incubation in the secondary antibody solution (as in wholemounts) for either three days at 4°C (thick sections) or one day at room temperature (thin sections). The subsequent procedures for preparing the thick sections (dehydration, clearing, mounting) were the same as the ones used in the wholemount protocol described above. The thin sections were first mounted on a chromealum/gelatin coated microscope slide where they were allowed to dry overnight before dehydration (distilled H_20 for 5 minutes, 50%, 70%, 90%, 96%, 2 x 100% ethanol for 3 minutes) and clearing (2 x 5 minutes in Xylene). The sections were mounted in Entellan (EMS, Hatfield, PA) under a coverslip.

Neurobiotin injections

For Neurobiotin labeling, we removed the beetle's legs and covered the stumps with wax. A thick layer of wax between the thorax and the abdomen immobilized the beetle. The animal was mounted on an adjustable holder with tape around the abdomen. The head was pulled out a few mm, bent down and waxed against the holder. A piece of head cuticle (either ventral or dorsal side) was cut out using a razor blade. Soft tissue and trachea around the brain were removed to reveal the target brain region, where a small incision to the neural sheet was made to facilitate the insertion of Neurobiotin crystals using the vaseline-covered tip of a sharpened borosilicate capillary. After washing with HBS, the head capsule was covered and the Neurobiotin was allowed to diffuse for 2-6 hours, depending on the target region. For backfilling of the antennal nerve (*AN*), we immobilized the beetle and cut the antenna from the proximal end of its flagellum. Neurobiotin crystals were then inserted into the open antennal stump. The stumps were covered with wax and the Neurobiotin was allowed to diffuse for ~24

hours. The dissected brains were placed into fixative (4% PFA, 0.25% glutaraldehyde and 2% picric acid in 0.1 M phosphate buffer) overnight at 4°C. The following day, the brains were rinsed with PBS for 4 x 15 minutes before incubating them in Cy3-streptavidin (1:1000; Jackson ImmunoResearch, West Grove, USA, cat number: 016-160-084) in PBT for three days. Subsequently, the brains were washed 6 x 20 minutes in PBT and 2 x 20 minutes in PBS before dehydration (50%, 70%, 90%, 96% and 100% ethanol), clearing (1:1 ethanol:methyl salicylate for 15 minutes; pure methyl salicylate for 35 minutes) and mounting in Permount.

Imaging

An LSM 510 Meta (Zeiss, Jena, Germany) confocal laser scanning microscope was used to image the brain samples. They were scanned with either a 633 nm HeNe laser (Cy5-fluorophore signal) or a 561 nm DPSS laser (Alexa-546 and Cy3-fluorophore signals) bidirectional and with a line average of 2. Single snapshot images were scanned unidirectionally with 2x or higher line average.

All brain samples were scanned with either a 10x water immersion (Plan Neofluar 0.45, Zeiss, with a correction factor of 1.14 due to differences between the refractive indexes of immersion and mounting media), 25x oil immersion (LD LCI Plan Apochromat 25x/0.8 Imm Corr DIC, Zeiss), or 40x oil immersion objective (Plan Neofluar 40x/1.3 Oil DIC, Zeiss). The step sizes (z-axis) of the optical slices varied from ~4-5 µm for image stacks taken to reconstruct the general layout of the brain and Neurobiotin injections or 1 µm for high resolution image stacks of brain regions. The resolution was defined either as 512 x 512 pixels (for reconstructing the general layout of the brain) or 1024 x 1024 pixels (Neurobiotin injections and brain regions) in the x-y axis.

Image stack processing and 3D reconstruction

All image stacks were processed using ImageJ (Fiji, RRID: SCR_002285; Schindelin et al., 2012) and Amira 5.3.3 software (FEI, Visualization Sciences Group, Oregon, USA; RRID: SCR_007353) and merged using the stitching plugin of FIJI in ImageJ (Preibisch et al., 2009) and the align tool of Amira. The image stacks were downsampled (1-2 μm^3 for image stacks of brain areas or 4 μm^3 for whole brain image stacks) in Amira prior to generation of 3D reconstructions. To improve clarity, all optical slices and maximum intensity projections shown in the figures were adjusted for brightness and contrast.

3D reconstruction of neuropils was performed in the segmentation editor in Amira where voxels of a certain structure of a grey image stack were first manually labelled in all three dimensions, from which the 3D structure was interpolated using the wrap tool (for details see el Jundi et al., 2010). Prior to visualization of specific brain areas and fibers using an intensity-based volume-rendering, the grey image stacks were masked using the module Arithmetic.

Nomenclature

To describe the neuropils and fiber bundles in the beetle brain, we used the nomenclature introduced by Ito et al. (2014). Thus, the insect brain can be divided into the cerebral ganglia (optic lobes and cerebrum) and gnathal ganglia (previously referred to as the subesophageal ganglion). For brain regions or fiber bundles that have not been described before we introduced new names following the rules of the nomenclature of Ito et al. (2014; see also Table 2). For the central-body neuropils, we used the terms commonly used in many insect species apart from e.g. *Drosophila*. Accordingly, the fan-shaped body is termed upper division of the central body, and the ellipsoid body is named lower division of the central body. For clarity, all

abbreviations for fiber bundles are italicized. All anatomical coordinates refer to the animal's body axis.

RESULTS

General layout of the brain

One brain of each species was chosen for comparison of the general layout of the dung beetle brain (Fig. 1). It consists of three clearly separated parts: (1) the optic lobes; (2) the cerebrum; and (3) the gnathal ganglia (GNG). Because both dung beetle species (the day-active *S. lamarcki* (Fig. 1A) and the night-active *S. satyrus*) have two separate dorsal and ventral pairs of compound eyes, the optic lobe in each brain hemisphere is conspicuously bifurcated into a dorsal and ventral part towards its distal end (Fig. 1C). The optic lobes are positioned laterally, relatively close to the retinae, and connect to the cerebrum via up to 1 mm long optic stalks (Fig. 1B-C). The GNG lies beneath the esophagus and is connected to the cerebrum ventrally via two circumesophageal connectives. Similar arrangements have been shown in many hemimetabolous insects, such as locusts (Bräunig and Burrows, 2004), the whirligig beetle (Lin and Strausfeld, 2012), and the red flour beetle (Dippel et al., 2016).

The layout of the "major neuropils" with well-defined boundaries is very similar between the diurnal and nocturnal species (Fig. 2A-E). These neuropil groups include the brain areas in the optic lobes, the anterior optic tubercles (AOTU), antennal lobes (AL), mushroom bodies (MB), central complex (CX) and the GNG. Due to the bilateral symmetry of the brain, each of these neuropils occurs as pairs with the only exception being some central-complex neuropils. As in other insect species described so far, anti-synapsin immunolabeling of the dung beetle brain results in specific staining of synapse-rich regions (Fig. 2F). All other regions with little or no synapses, i.e. fiber bundles and glial processes, basically lack any staining, thus appearing dark in the confocal images.

The remaining brain volume is covered by the neuropils of the cerebrum with more ambiguous boundaries. As most of these neuropils cannot be separated based only on anti-synapsin staining we needed to reconstruct the fiber bundles of the cerebrum as landmarks. In the following, we will first describe the brain areas with well-defined boundaries before characterizing the neuropils of the cerebrum with less distinct boundaries.

Optic lobes

The optic lobes are the first processing stages for visual signals. The layouts of the optic lobes in both dung beetle species are clearly homologous (Fig. 3A-D). The distalmost neuropils in the optic lobe are the laminae in which the optic cartridges are clearly visible in both species based on the anti-synapsin staining (Fig. 3E). The somewhat unusual arrangement with two compound eyes on each side of the beetles' head results in a dorsal (DLA) and a ventral lamina (VLA). With anti-5-HT staining several layers in the DLA and VLA could be defined in both species (Fig. 3E,F). The laminae are separated from the second optic lobe neuropil, the medulla (ME), by the first optic chiasms (Fig. 3A-D). The ME consists of two subdivisions, the distally located outer medulla (OME) and proximally to it, the inner medulla (IME). Both neuropils are separated by a relatively wide serpentine layer (SPL; Fig. 3C-D) devoid of anti-synapsin staining. In both species we defined in total 11 layers in the ME, with layer eight being the SPL (Fig. 3G-J). Seven layers could be characterized in the OME and three layers in the IME. The segregated connections of the first optic chiasms to the ME and the occasional disordered appearance at the medial point of the OME and IME (Fig. 3C,D, arrows) indicated that each ME could be further divided into a ventral and dorsal half, similar to what has been shown in the whirligig beetle (Lin and Strausfeld, 2012). However, since the ventral and dorsal halves

were clearly fused, and a distinct boundary was missing, we decided to treat the OME and IME as undivided structures. The IME is proximally flanked by the lobula complex (Fig. 3A,B). The anterior-most lobula complex neuropil is the pyramidical shaped lobula (LO), which consists of at least two parts, the outer lobula (OLO) and the inner lobula (ILO). Close to the LO, on the posterior side of the optic lobe lies a neuropil that is known to be a crucial center for motion vision in many insect orders (Strausfeld, 2005), the lobula plate (LOP). Although the LOP mostly appeared as a single contiguous structure, horizontal optical sections taken from its dorsal region indicate the presence of a layered organization (Fig. 3C3,D3 insets). The smallest of the optic lobe neuropils is the accessory medulla (AME), located close to the anteromedial edge of the ME, adjacent to the OLO.

The only prominent differences between the diurnal and nocturnal dung beetle optic lobes presented in Fig. 3 could be found in the laminae. Both DLA and VLA are much larger in the nocturnal species than in the diurnal counterpart (Fig. 3A-D). Even though the body of the tested diurnal specimen was larger (thorax width: 2.08 cm; head width: 1.29 cm) than that of the nocturnal individual (thorax width: 1.70 cm; head width: 1.10 cm) the combined absolute volume of DLA and VLA proved to be ~2-fold larger in the latter (*S. lamarcki*: $19.1 \cdot 10^6$ µm^3; *S. satyrus*: $41.3 \cdot 10^6$ µm^3). Interestingly, the absolute volumes of the ME (OME and IME; *S. lamarcki*: $27.6 \cdot 10^6$ µm^3; *S. satyrus*: $23.4 \cdot 10^6$ µm^3) and the lobula complex (OLO, ILO and LOP; *S. lamarcki*: $9.9 \cdot 10^6$ µm^3; *S. satyrus*: $7.9 \cdot 10^6$ µm^3) were similar. Consequently, ratios taken between the LA and ME (LA/ME; *S. lamarcki*: 0.69; *S. satyrus*: 1.76), and LA and lobula complex (LA/lobula complex; *S. lamarcki*: 1.93; *S. satyrus*: 5.25) were ~2.5-fold larger in the nocturnal dung beetle than in its diurnal counterpart. Further differences could be found in the structural appearance of the laminae. While in the diurnal species the appearance of laminae is more uniform, the laminae in the nocturnal species consist of a conspicuous, additional unstained layer (Fig. 3F) that might consist of neural fibers. Consequently, while the DLA and VLA of the diurnal species consists of three layers (Fig. 3E; VLA not shown here), we could define four layers (with layer three lacking anti-synapsin immunoreactivity) in the nocturnal species. The most striking finding, however, was the existence of a clearly separable region in the DLA of the nocturnal dung beetle, a large dorsal rim area of the lamina (LADRA; Fig. 3A-D), which could not be distinguished in the diurnal species. In other insects, this region is associated with polarization vision (Labhart and Meyer, 1999) and was separated from the remaining DLA by a distally located notch (Fig. 3D, arrowhead). In contrast to the remaining DLA, the LADRA exhibits three more layers, and therefore, at least seven layers (Fig. 3F).

Anterior optic tubercle

Some of the most prominent outputs from the optic lobe project via the optic stalks to the cerebrum and arborize in the anterior optic tubercle (AOTU; Fig. 4). In both species, the AOTUs are located at the dorsolateral edge of the anterior cerebrum, close to the proximal ends of optic stalks. Although the AOTU was discernible from the anti-synapsin staining already in low magnification and resolution (see Fig. 2F2), it was not clear exactly where the boundary between its medial end and the rest of the cerebrum is. Tracer injections into the dorsal edge of the medulla (DME) were used to stain the neurons projecting to the AOTU. In the diurnal beetle, the anterior optic tract (*AOT*) and the neurons' synaptic outputs in the AOTU were stained (Fig. 4A1-A4) and showed dense and clearly separated arborizations in the lateral region of the AOTU, which could be divided into six subdivisions of the lower unit (Fig.4A2-A4). The neuropilar architecture in the lateral region of the AOTU in the beetle therefore seem to be similarly complex as the one found in honey bees (Zeller et al., 2015), and we accordingly termed it the lower unit complex (LUC). An area posteromedially to the LUC was also stained with scarce but varicose arborizations extending close to the dorsal edge of the protocerebrum.

Due to the similarity to the bumble bee's AOTU branching pattern (Pfeiffer and Kinoshita, 2012), we defined this area as the upper unit of the anterior optic tubercle (UU).

The AOTU divisions defined according to the tracer stainings could be confirmed in the anti-synapsin stainings (Fig. 4B-C). In both species, the six subunits of the LUC were detached from the UU and connected only via the *AOT*. Although the boundaries for subdivisions III-VI in the diurnal beetle were not easily distinguishable our demarcation still roughly corresponded to the location of subdivisions in the tracer injection (Fig. 4B). In the nocturnal beetle, the boundaries for all divisions were clear and the subdivisions of the LUC could be demarcated without tracer injections (Fig. 4C). The anti-synapsin staining also showed that in both species the UU extends ventrally and merges into the superior protocerebrum.

3D reconstructions of the diurnal and nocturnal AOTUs showed that both LUC and UU are structured in a similar fashion (Fig. 4D-E). Although the shapes of the LUCs are clearly different between the two species, the position and proportional sizes of their subdivisions are roughly the same. Accordingly, only the subunits IV and VI appeared to be larger in the nocturnal than in the diurnal beetle (compare Fig. 4D and 4E) when comparing the volumes of the reconstructed AOTU subunits normalized to the overall AOTU volume between the species (LUC subunit IV: *S. lamarcki*: 0.012 vs. *S. satyrus*: 0.022; LUC subunit VI: *S. lamarcki*: 0.005 vs. *S. satyrus*: 0.014).

Lateral complex

From the AOTUs, visual signals are relayed to the lateral complex (LX; Fig. 5), a group of neuropils that lie on either side of the brain, roughly ventral to the MB and anterolateral to the CX. By combining anti-synapsin with anti-5-HT staining the LX could be divided into three neuropils: the lateral accessory lobe (LAL), the gall (GA), and the bulb (BU). The LAL was further subdivided into upper (ULAL) and lower LAL (LLAL) according to the LAL commissure (*LALC*), which mediolaterally enters the LAL (Fig. 5A). The GA, which lies at the anterior edge of the LAL, and is partially engulfed by the ULAL, was found to consist of three clearly distinguishable blob-like subunits (Fig. 5A-C). In accordance with *Drosophila*, these subunits were termed the ventral GA (VGA), the dorsal GA (DGA), and the GA tip (GAT; Wolff et al., 2015). The BU is a neuropil where AOTU neurons form microglomerular contacts with CX cells in many insects, such as locusts (Träger et al., 2008), bees (Held et al., 2016; Mota et al., 2016), ants (Schmitt et al., 2016), fruit flies (Seelig and Jayaraman, 2013), and monarch butterflies (Heinze et al., 2013). In the dung beetle brain, the BU lies at the posterior side of the ULAL (Fig. 5B-C) and is faintly stained by anti-synapsin in both species, but was still detectable due to its close association with the brightly stained (anti-5-HT) isthmus tract (*IT*; Fig. 5A3,A4 insets), and the tract originating from the ipsilateral AOTU and terminating in the BU, the tubercle-to-bulb tract (*TUBUT*; Fig. 5A,D,E).

The LAL comprises by far most of the LX volume (Fig. 5B). In both species, it is clearly delineated on its anterior side where it is flanked by the posteromedial edge of the AL. However, towards posterior, the LAL boundaries become gradually more ambiguous ventrally and laterally in the anti-synapsin staining (Fig 5A). We therefore used the 5-HT staining to define the ventral and lateral boundaries of the LLAL, in the same way as it has previously been done for the monarch butterfly brain (Heinze and Reppert, 2012; Fig. 5A insets). To demarcate the rest of the boundaries we used fiber bundles as landmarks (Fig. 5D-E), which have previously been described in the silkworm moth (Iwano et al., 2010), monarch butterfly (Heinze and Reppert, 2012), and the fruit fly *Drosophila* (Ito et al., 2014). Another major landmark were the MBs, which were used to define the superior boundaries of the ULAL (Fig. 5D,E).

Central complex

Closely associated to the LX is the central complex (CX), located at the midline of the brain. As in other insects, the CX of dung beetles consists of four neuropils, the central body (CB) formed by its lower (CBL) and upper division (CBU), the paired noduli (NO), and the protocerebral bridge (PB; Fig. 6A-B).

The most anterior neuropil is the sausage-like CBL. In both dung beetle species, it was characterized by faint anti-synapsin labeling that alternated to form a slice-like appearance (Fig. 6C). No indications of horizontal layering was found. Anti-5-HT staining also clearly showed the connection between the CBL and the *IT* via which the CBL receives synaptic input from the BU (el Jundi et al., 2015b). Right posterior to the CBL lies the larger division of the CB, the CBU. In both species, the CBU could be divided into at least four horizontal layers (I-IV from dorsal to ventral) on the basis of anti-synapsin staining (Fig. 6D). Except for the layer IV, no obvious signs of slice-like organization could be observed. Although there were some variations in the staining intensity between species, anti-5-HT consistently stained CBU layers I, III and IV in the diurnal and nocturnal beetle species. The relatively thin layer II, in turn, showed no immunoreactivity to anti-5-HT, but instead was brightly stained with anti-synapsin. The major characteristic of layer III was its irregular appearance in synapsin labeling caused by the penetrations of several tracts. Especially at the lateral edges of the posterior CBU, layer III was occasionally relatively difficult to separate from layer IV lying ventrally to it. Towards the anterior CBU, however, layer IV started to show more distinct structure with faint indications of slice-like units.

Ventral to the CB lie the paired NO, the two spherical neuropils completely devoid of anti-5-HT immunoreactivity. They could be divided into four layers based on the anti-synapsin staining (Fig. 6A-B, E). The last of the CX neuropils is the unpaired elongated, arch-like PB located relatively close the posterior margin of the brain. Although the PB mostly appears as a single fused structure, each of its halves could be divided into eight slices based on somewhat regularly appearing grooves or dark boundaries (Fig. 6F), thus, following the number of slices observed in locusts and monarch butterflies (Williams, 1975; Heinze and Homberg, 2008; Heinze et al., 2013).

Antennal lobes and AMMC

The ALs, which are the first integration centers for olfactory information, are the largest neuropils in the cerebrum and occupy the anterolateral regions in the brain, directly posteromedial to the antennae. The ALs are closely associated to the antennal mechanosensory and motor centers (AMMC), which are located posterior to the AL and have relatively ambiguous boundaries. Since the AMMC receives direct input from a group of fibers in the antennal nerve, the boundaries could be distinguished by performing two anterograde stainings of the AMMC with mass injections of Neurobiotin into the dung beetle's antennae. The results exhibited a relatively complex structure for the AMMC with two medially extending projections (Fig. 7A,B). An additional interesting observation was that a thick bundle of antennal nerve fibers run past the AL and AMMC, all the way to the GNG (Fig. 7A,B). As in other insects, the AL consists of glomeruli (Fig. 7C-H) that are arranged around the AL hub (ALH; Fig. 7F3,I3). Olfactory receptor neurons project from the antennae via the antennal nerve into the ALH, from where they then innervate about 83 (diurnal, Fig. 7D-F) or 86 (nocturnal, Fig. 7G-I) glomeruli. When comparing a male and a female AL of the same species, we were able identify the same glomeruli in both sexes without any obvious evidence for sexual dimorphism (data not shown). In contrast, when comparing the diurnal and nocturnal ALs (both male; Fig. 7D-I), no homologous glomerulus could be identified with the exception of one large glomerulus lying at the ventromedial edge of the AL in both species (Fig. 7D-I). This glomerulus, which was termed as the accessory glomerulus (AGL), was not only characterized

by its size, shape and slightly isolated location but also by a thick fiber entering it from its dorsomedial corner (Fig. 7F3,I3). Interestingly, the antennal backfills did not stain the AGL (Fig. 7C). Finally, the ALH gives rise to the AL tracts (*ALT*) that exit the AL from ventromedial and transmit signals to higher order olfactory processing sites.

Mushroom bodies

The MB in dung beetles is structured in a similar fashion as in other insects (Strausfeld et al., 2009; Fig. 8). In each hemisphere, the cell bodies of the Kenyon cells are packed into two groups at the dorsoposterior edge of the central brain. Directly anterior to the cell body layer Kenyon cell dendrites form a single ovoid calyx (CA) brightly stained with anti-synapsin (Fig. 8A). As tracer injection experiments stained only fibers projecting from the AL to the CA but never from the optic lobes to the CA (see below), as found in many insects (Ehmer and Gronenberg, 2002; Sjöholm et al., 2005; Lin and Strausfeld, 2012; Kinoshita et al., 2015; Stöckl et al., 2016a; Vogt et al., 2016) it seems as the MBs only receive direct olfactory input in dung beetles. The large synaptic complexes formed by the AL projection neurons and the Kenyon cells in the CA are nicely visible in the anti-synapsin staining (Fig. 8A1). Beneath the CA two Kenyon cell axon bundles showing strong anti-5-HT immunoreactivity project towards anterior through the pedunculus (PED; Fig. 8B1; see also the inset in 8B1 for the two groups of Kenyon cell bodies in the posterior brain). In both species, the PED was found to consist of at least three coaxial layers (Fig. 8A2-C2, insets). It extends all the way from the posterior surface of the brain, past the coronal midline to the anterior half of the brain, before it turns medially and bifurcates into the ventral lobe (VL) and the medial lobe (ML), the latter extending in front of the CB (Fig. 8A-C). Especially based on the anti-5-HT staining distinct laminae within the PED, VL and ML could be defined. Similar to the MB in *Tribolium castaneum* (Zhao et al., 2008; Binzer et al., 2014), an inner lamina that bifurcates into VL- and ML-sublobes could be separated from an outer region that in dung beetles lacks any 5-HT staining. The outer region was defined as the medial γ lobe (MγL) and the vertical γ lobe (VγL), (Fig. 8A3,A4,C3,C4,D,E) in line with the findings in *Tribolium castaneum* (Zhao et al., 2008; Binzer et al., 2014). The sublobes stained with anti-5-HT were determined as the α,α' lobe (α,α'L) in the VL, and β,β' lobe (β,β'L) in the ML (Fig. 8B3,B4,C3,C4,D,E).

Central adjoining neuropils

A large proportion of the overall synaptic neuropil volume is occupied by a group of cerebral neuropils adjoining the central neuropils described above. A common characteristic of these central adjoining neuropils (CANP) is that the boundaries of many of them are often very ambiguous, and thus, difficult to demarcate. With the aid of GAL4-driver lines in *Drosophila*, or several staining techniques, and developmental information in other insects, these neuropils can be described in detail (Heinze and Reppert, 2012; Ito et al., 2014; Bressan et al., 2015).

One of the best known regions within the CANP is the lateral horn (LH), which is, besides the MB, the second main projection site of the olfactory projection neurons originating in the AL. To describe this area in the dung beetle central brain we first performed Neurobiotin mass injections into the AL and the MB. When injected into the AL Neurobiotin stained in total four *ALTs* (Fig. 9A-C). Three of the tracts are the ones typically found in other species: the *lALT*, *mALT*, and *mlALT*. Due to its high resemblance to a corresponding *ALT* described in *Drosophila* (Tanaka et al., 2012a; b) and a moth species (Ian et al., 2016a), the fourth tract running between *mALT* and *mlALT* was named as the transverse *ALT* (*tALT*). The largest *ALT* was the *mALT*, which was also characterized by the presence of a brightly anti-5-HT-stained fiber (not shown). All of the four *ALT*s made connections within the cup-like LH at the very lateral edge of the superior protocerebrum (Fig. 9A-C). When Neurobiotin was injected into

the CA it stained only one of the *ALT*s, the *mALT* (Fig. D-F), resulting in incomplete staining of the LH, suggesting that neurons comprising different tracts innervate different subregions in the LH. In addition, the whole MB was stained, as well as a thin bundle of fibers connecting the α,α'L and LH (Fig. 9D-F).

To further define the CANP we reconstructed all major fiber bundles of the diurnal dung beetle brain. Together with the neuropils described above these fiber bundles were used as landmarks to determine the CANP boundaries similar to what has been shown in the *Drosophila* brain (Ito et al., 2014). The reconstruction of the fiber bundles was based on the anti-synapsin stainings. Because in most cases anti-synapsin does not stain any tracts and fibers, they appear as black regions in the confocal images. Overall, 21 fiber bundles, including ten tracts, seven commissures, two fascicles, and two fiber systems were labeled and reconstructed (Fig. 9G-J). The CANP could be divided into 13 paired and 4 unpaired neuropils (Fig. 10), which also included the GNG (Fig. 10E). The CANP were divided into super-categories in accordance with Ito et al. (2014): the superior neuropils (SNP), the ventrolateral neuropils (VLNP), inferior neuropils (INP), ventromedial neuropils (VMNP), and the periesophageal neuropils (PENP).

Superior neuropils

The most dorsal group of the protocerebrum, the SNP, consists of three neuropils: the superior lateral protocerebrum (SLP), the superior intermediate protocerebrum (SIP), and the superior medial protocerebrum (SMP; Fig. 10F, 11A). The SNP are laterally flanked by the LHs. The SMP and SIP appear anteriorly at the level of the AOTU (Fig. 10F, 11A), to which the SIP is closely connected and engulfs the associated *TUBUT*. While the SIP has its posterior borders posterior to the VL of the MB, the SMP extends further through the brain and has its boundaries anterior to the CA (Fig. 10F11). The SLP appears right posterior to the AOTU, dorsolaterally flanking the SIP, and extends towards the posterior brain surface where it has its posterior boundaries lateral to the CA (Fig. 10F11,F12). At its anterior side, the SLP is relatively easily distinguishable from the LH based on anti-synapsin labeling (Fig. 10C, 10F4). At the level of the posterior end of the VL, however, the boundaries become less distinct. Roughly at this level, the boundaries between the SLP and SIP, and SLP and LH are defined with the help of two tracts, the superior lateral protocerebral tract (*SLPT*) and the lateral superior medial protocerebral tract (*lSMPT*; Fig. 9G-J). The *SLPT* consists of three branches, two of which flank the anterior edge of the LH dorsally and ventrally, while the third lies at the anterior boundary between the SLP and SIP. The *SLPT* and *lSMPT* converge at the level where the anterior edge of CBL starts. The *lSMPT* runs through the ventromedial SLP and terminates in the SMP close to the posterior edge of the SIP. Laterally, the *lSMPT* runs in between of the LH and ventrolateral protocerebrum. The posterolateral boundary between LH and SLP was defined by the point where the inferior optic tract (*IOT*), which originates form the ipsilateral optic lobe (posteroinferior to the *AOT*), laterally enters the brain, superior to the ventrolateral neuropils. Approximately at this level, the fibers of the *mALT* project into the LH. The rest of the medial and lateral boundaries of the SLP and SMP, respectively, were defined according to the position of the lateral edge of the superior fiber system (*SFS*).

Ventrolateral neuropils

Ventral to the SNP lie two paired VLNP: the ventrolateral protocerebrum (VLP) and the posterior lateral protocerebrum (PLP; Fig. 10A, 10F3-F6,11B). At the anterior side of the brain the VLP begins posterior to the AL, at the lateral edge of the SIP. The anterior edge of the VLP is roughly at the level of the anterior boundary of the SLP. The borders of the VLP are relatively well-defined based on the anti-synapsin signal. Furthermore, it stands out from the rest of the brain due to highly enriched 5-HT-immunoreactive arborizations (results not shown). At its

dorsal end, VLP was separated from the SNP and the LH also by using two tracts, the *lSMPT* and *IOT*, as landmarks. Medially, this region is defined by the LAL, the epaulette (EPA, see below) of the ventromedial neuropils, and the PED. At its ventroposterior end, VLP is neighbored by the PENP (Fig. 10A,F6). The posterior half of the VLNP, the PLP, is separated from the VLP by the great commissure (*GC*). Unlike the VLP the boundaries for the PLP were more difficult to demarcate, especially at its ventral side where it is flanked by the posterior slope (PS) and the PENP. Here, the boundaries were demarcated by the clamp-tritocerebral tract (*CTT*), which projects from the ventral CL (lateral to the *LEF*) to the lateral edge of the PENP. Medially, the boundaries were defined using the lateral equatorial fascicle (*LEF*) and the PED. The dorsal boundary was largely determined by the *IOT*, but close to the posterior side the separation between the PLP and the SLP was based solely on differences in the anti-synapsin staining. Posteriorly, the PLP ends at the posterior cell body rind, next to the posterior optic commissure (*POC*).

Inferior neuropils

The INP lie medio-ventrally from the SNP, and are laterally flanked by the VLNP (Fig. 11C). These neuropils occupy the space superior to cavity above the CX, around the ML and the PED. The most anterior neuropil is the crepine (CRE), which extends to the anterior edge of the brain and wraps around the ML. It is mostly demarcated by surrounding glial processes. Dorsally CRE adjoins the SIP and the SMP (Fig. 10F1,F2). From the SIP it could be separated by its more intense anti-synapsin staining (Fig. 10F1). Ventrally the CRE ends next to the dorsomedial edge of the LAL. The lateral neighbor of CRE is the clamp (CL), which surrounds the dorsal and medial sides of the PED all the way to the CA (Fig. 10F5-F11). At this level the CL also meets the superior PLP commissure (*sPLPC*). Dorsally it is separated from the SNP by the *SFS*, while dorsomedially its boundary is defined by a plane drawn between the *SFS* and the lateral edge of the CBU. From its laterally neighboring VLNP the ventrolateral CL is separated by the *LEF*, which together with the *CTT* and medial equatorial fascicle (*MEF*) also defines the ventral boundary. The dorsolateral boundary, in turn, was defined according to a plane interpolating the PED and the *IOT*. Medially the CL is demarcated by the *mALT* and the CB. The two other members of the INP are the unpaired, midline crossing antler (ATL) and inferior bridge (IB), which lie dorsal and ventral to the posterior CB, respectively (Fig. 10F8,F9). The ATL is mostly demarcated by surrounding glial processes. However, at its anterior end it fuses with the SMP, from which it was differentiated by its slightly different pattern of anti-synapsin staining (Fig. 10F8). The ATL was also closely associated to the superior PLP commissure (*sPLPC*) at its posterior end. On its ventral side, at the posterior end the ATL makes two connections to the IB (Fig. 10F11). Close to the brain midline the IB is also easily distinguishable. Anteriorly it is flanked by the gorget (GOR) of the VMNP, which stands out from the IB by its brighter anti-synapsin signal (Fig. 10F7,F8). The anterior edge of IB is also neighbored by the minor optic commissure (*MOC*), which is a relatively thin bundle of fibers that runs right posterolateral to the GC and merges to it ventromedially. Laterally the IB is demarcated by the *IFS*. Ventrolaterally it is contiguous with the posterior slope (PS) of the VMNP (Fig. 10F8-F12). The boundary between the two is defined according to a plane defined by the lateral edge of the PED and the midpoint of the *IFS*. Posteriorly the IB extends all the way to the level of CA (Fig. 10F12).

Ventromedial neuropils

The VMNP also consist of four neuropils, all of them paired: GOR, PS, EPA, and the vest (VES; Fig. 11D). The GOR is a cantilever-like neuropil that lies just below the NO (Fig. 10F7). Its anterior boundary is roughly aligned with the anteriormost surface of the GC, while its

posterior boundary lies close to the level where *mALT* and *MEF* meet. Both laterally and ventrally the GOR is flanked by the VES, from which it is discriminated by its slightly brighter anti-synapsin staining (Fig. 10F7,F8). The VES lies ventral to the ML, next to the esophageal foramen. It stretches from the level where the posterior limit of the AL lies to the level of the GC. It is distinguishable by a thin wrap that it makes around the *mALT* running above it (Fig. 11D). Its dorsolateral boundary, which is flanked by the LAL and the EPA, is demarcated by a plane that is interpolated between the *mALT* and the *IFS*. The ventrolateral boundary is defined by the *IFS*. Ventrally the VES is neighbored by the periesophageal neuropils (PENP; Fig 10A,F2-F5). The boundary between the two roughly corresponds to the line drawn between the ventral limits of the *IFS*. The posterior neighbor of the VES is the PS. In anterior-posterior direction it stretches from the level of the GC to that of the POC. In many parts it is fused with its dorsolateral and ventrolateral neighbors, the PLP and the PENP (Fig. 10F7-F11). These three could be separated by using the diagonal line created by the *CTT*. On the dorsal side, the PS is separated from the CL by a plane created by the *MEF* and the *LEF*. With its dorsomedial neighbor, the IB, the PS is contiguous and lacks a clearly distinguishable boundary (Fig. 10F7-F12). To delineate this boundary we used the plane that can be drawn via the lateral edges of the dark regions created by the PED and the *MEF*. The ventral boundary of the PS was defined in the same way as in the case of the VES. In addition, the inferior PLP commissure (*iPLPC*), which terminates in the ventral PLP and is inferior to the *POC*, was used to separate the ventrolateral side of the PS from the neighboring PENP. The EPA is contiguous with the LAL, and its anterior boundary is defined by the *mlALT*. On its posterior end its boundary was determined by the GC, in front of its posterior neighbor, the PS (Fig. 10F5,F6). From its medial neighbor, the VES, the EPA is distinguished by its less bright and slightly more irregular appearance with anti-synapsin labelling. On the lateral side, where EPA is flanked by the VLP, the boundary roughly corresponds to a plane interpolating the lateral surfaces of the PED and the *IFS*. *IFS* is also used as a landmark to delineate EPA's ventral boundary. Finally, the EPA is dorsally defined by the PED on its anterior side and by the CL on its posterior side (Fig. 10F4-F6).

Periesophageal neuropils

The most ventral group is formed by the PENP (Fig. 10A-D,F and 11E). The only clearly separated structure that could be distinguished were the AMMCs (Fig. 7A,B, 10A,B, 10D,F3-F6), which lie on the lateral sides of the brain, partially engulfed by the remaining PENP. The PENP extends all the way from the anterior edge of the brain to the level of the *POC* (Fig. 10F12). Dorsally it is delineated by the *IFS*, *CTT*, and the *iPLPC*. Ventrally the PENP becomes narrower and ultimately gives rise to the CEC that connect to the GNG.

DISCUSSION

One main aim in neuroethology is to understand how brain architecture reflects the behavioral repertoire displayed by an animal. In this study, we present the layout of the brains of two closely-related dung beetle species (Forgie et al., 2006), the diurnal *S. lamarcki* and the nocturnal *S. satyrus*. As these beetles share a similar lifestyle and natural habitat (but are active at different times of day), our findings provide an important framework for comparative neurological studies on sensory ecology in insects active at different times of day. The detailed descriptions of different brain regions, including many of the major fiber bundles, also provide a useful reference for characterizing the neuronal network of different behaviors in dung beetles, including olfactory and celestial compass orientation.

Comparison between diurnal and nocturnal dung beetles

Overall, the brains of the diurnal and nocturnal dung beetle species have a very similar neuroarchitecture. Brain regions that are considered to be multimodal higher-order neuropils, such as the mushroom bodies or the central complex, are basically indistinguishable between the species, suggesting that information close to the motor output is processed in a similar way in both species (Figs. 6 and 8). A slight difference was found in the 5-HT-immunoreactivity in the upper division of the central complex (CBU). While layer I was strongly stained in the diurnal species, this layer showed less intense 5-HT-immunoreactivity in the nocturnal species. However, to draw firm conclusions, this requires quantitative assessment that needs to be controlled for potential circadian effects (day-active beetle brains were dissected during their subjective day, while the night-active beetle brains were dissected during their subjective night).

To improve sensitivity to light, night-active insects typically have much larger compound eyes than their day-active counterparts (Warrant, 2008; Warrant and Dacke, 2011). This difference in eye design is obvious among the dung beetles (Byrne and Dacke, 2011). The network in the primary visual integration centers in the brain, the optic lobes, have also been demonstrated to support a higher sensitivity for dim-light vision (Greiner et al., 2004; Stöckl et al., 2016b). Because of the different activity periods of the two beetle species presented in this paper, we thus expected clear differences in the layout of their optic lobes. We indeed found clear size difference of the optic lobe neuropil volumes, especially regarding the first integration centers, the laminae (Fig. 3). Thus, eye size correlates with the size of the optic lobe in dung beetles in the same way as has been shown in ants (Gronenberg and Hölldobler, 1999). A further comparison of the size ratio between laminae/medulla illustrates that this ratio is much larger in the nocturnal species (~2.5-fold) than in its diurnal counterpart (Fig. 3). This suggests that in nocturnal beetles spatial summation is taking place to a higher degree between the laminae and medulla, a strategy commonly utilized to increase sensitivity at dim light (Warrant and Dacke, 2011).

Another distinct difference is the existence of a very large dorsal rim area of the lamina (LADRA) in the nocturnal species that could not be identified in the diurnal species. This region is known to house the synaptic outputs of photoreceptors from the dorsal rim area (DRA) (Blum and Labhart, 2000; Homberg and Paech, 2002; Schmeling et al., 2015), a specialized eye region that mediates polarization vision in many insects (Labhart and Meyer, 1999; Mappes and Homberg, 2004; Wernet et al., 2012) including the dung beetles (Dacke et al., 2014). Both dung beetle species rely on polarized light for orientation (Dacke et al., 2011; el Jundi et al., 2014b), but weight this cue differently: the night-active species relies on it as its primary orientation reference while the day-active species ranks it lower than the sun (el Jundi et al., 2015b). Accordingly, half of the dorsal eye of crepuscular and nocturnal dung beetles is equipped with polarization-sensitive photoreceptors of the dorsal rim area (Dacke et al., 2003b) while in the day-active species only a very small DRA has been localized (Dacke, unpublished). Taken together, the size of the DRA and thus, the cue hierarchy is reflected in the lamina with a large LADRA in the night-active species allowing it to use a wide-field stimulus as orientation cue at very dim light conditions.

The antennal lobes (AL) are large in both species, suggesting that, in general, dung beetles strongly rely on olfactory cues for many behaviors, such as finding a specific type of dung, animal or plant (Midgley et al., 2015; Mansourian et al., 2016) or for being attracted to pheromones of the male specimen (Tride and Burger, 2011; Burger, 2014). In the two species investigated here, the difference in activity period does not substantially affect the number of AL glomeruli (about 83 in the diurnal species; about 86 in the nocturnal species). In moths and butterflies however, the glomeruli sizes were different between nocturnal and diurnal animals, suggesting a different investment in processing of olfactory cues (Montgomery and Ott, 2015;

Stöckl et al., 2016a). Whether this is also the case in dung beetles requires a careful allometric analysis of body parts (antennae, head size) and different brain areas combined with behavioral choice experiments in both species. Taken together, even though the AL of both dung beetle species are somewhat different, a clear conclusion about the effect of activity period cannot easily been drawn here.

Comparison between dung beetles and other insects

Optic lobes

The general layout of the optic lobes follows the one described in many other insects (Strausfeld, 1976, 2012; Ito et al., 2014), including beetles (Dreyer et al., 2010; Lin and Strausfeld, 2012; Kollmann et al., 2016). It consists of the outermost laminae, the medulla and lobula complex (Fig. 3). Due to the existence of four eyes (two of each side of the head), the laminae (and also medullae) are split into a dorsal and ventral lamina (dorsal and ventral medulla), similar to what has been shown in the whirligig beetle (Lin and Strausfeld, 2012). In those aquatic insects, however, the ventral eyes are facing downwards towards bodies of water while dorsal-eye input seems to be important for landmark orientation. Accordingly, the authors found neurons that run from the dorsal medulla into the mushroom bodies (Lin and Strausfeld, 2012). In dung beetles, we did not find this connectivity but instead found neurons that project from the dorsal medulla into the anterior optic tubercle (AOTU). These neurons have been described in many insects such as ants, bees and locusts (Homberg et al., 2003a; el Jundi et al., 2011; Mota et al., 2011; Pfeiffer and Kinoshita, 2012; Zeller et al., 2015; Schmitt et al., 2016), and are known to play a role in celestial compass orientation. Therefore, in dung beetles, signals from the dorsal lamina and medulla seem to be important for celestial compass orientation while the input from the ventral eyes could, for example, play a crucial role for body stabilization based on optic flow information when flying or rolling a dung ball.

While we were able to find a LADRA in the nocturnal dung beetle species, we were not able to find the dorsal rim area of the medulla (MEDRA). This region has been described in *Drosophila* (Fortini and Rubin, 1991; Weir et al., 2016), bees (Pfeiffer and Kinoshita, 2012; Zeller et al., 2015), ants (Schmitt et al., 2016), and locusts (Homberg and Paech, 2002; el Jundi et al., 2011; Schmeling et al., 2015). However, in *Drosophila* the MEDRA seems to be less separable from the remaining medulla without the help of transgenic flies or tracer-injection experiments into the LADRA (Fortini and Rubin, 1991) and this could be the reason why we did not find it in dung beetles yet. Similar to what has been shown in many insects, the lobula of the lobula complex of the dung beetle brain can be divided into different subunits (or layers). Here we found two subunits in the beetle brain, similar to the sphinx moth *Manduca sexta* (el Jundi et al., 2009). In other insects, the lobula has been reported to consist of either one (fruit flies: Rein et al., 2002; honeybees: Brandt et al., 2005) or up to four subunits (locusts: Kurylas et al., 2008), based on anti-synapsin staining. This variance in lobula subunits may suggest that the lobula has a variety of functions that are specialized to different insect orders.

Finally, we were able to define the accessory medulla (AME) in the beetle brain. This brain region has been described in all insects so far, with the exception of bees and wasps, and, at least in cockroaches and *Drosophila*, has been established as the circadian pacemaker in the insect brain controlling locomotor activity (Homberg et al., 2003b; Reischig and Stengl, 2003; Helfrich-Förster, 2004). Whether this function is also true in dung beetles has yet to be revealed.

Anterior optic tubercle

The anterior optic tubercle (AOTU) is a high-order visual neuropil, consisting of a varying number of subunits across species (Homberg et al., 2003a; Strausfeld and Okamura, 2007; el Jundi et al., 2010; Heinze and Reppert, 2012; Montgomery and Ott, 2015; Zeller et al., 2015; Montgomery et al., 2016). However, two of the subunits, the lower and upper unit, seem to be functionally conserved in all species investigated so far. The lower unit has been shown to specifically receive information from polarization sensitive neurons, whereas the upper unit is involved in the processing of unpolarized visual signals (Homberg et al., 2003a; Pfeiffer et al., 2005; Mota et al., 2011, 2013; Pfeiffer and Kinoshita, 2012; Zeller et al., 2015).

In the dung beetle AOTU, the upper unit of the anterior optic tubercle (UU) appeared homologous to its counterparts in other species. However, what could be regarded as the lower unit in the AOTU of dung beetles was found to be a complex consisting of at least six subunits (LUC). Similar complexity has previously been described in the LUC of the honeybee AOTU (Zeller et al., 2015). In addition, the branching patterns of neurons in the lower unit of the AOTU in monarch butterflies are very distinct and restricted to certain domains suggesting a similar subcompartmentalization (Heinze et al., 2013). As suggested by Zeller et al. (2015) and Heinze et al. (2013) the subcompartmentalizations of the lower unit/LUC might be a result of spatial mapping of different projection neurons between the AOTU and the bulb (BU).

Lateral complex

The lateral complex (LX) houses neuropils that are closely associated with neuronal networks comprising the central complex (CX) (Strausfeld, 1976; Heinze and Homberg, 2008). For instance, celestial compass information from the AOTU is sent to the bulbs (BU) of the LX, where the tubercle-to-LAL (TuLAL; in dung beetles, the fibers belonging to the *TUBUT*, Fig. 5) projection neurons provide synaptic input to GABAergic tangential neurons of the lower division of the central body (CBL; Pfeiffer and Homberg, 2014). The large synapses between these neurons form a conspicuous microglomerular complex, a feature that seems to be conserved across insects (Träger et al., 2008; Heinze and Reppert, 2012; Pfeiffer and Kinoshita, 2012; Seelig and Jayaraman, 2013; Held et al., 2016; Mota et al., 2016; Schmitt et al., 2016).

In dung beetles, only one bulb (BU) was found in the LX (Fig. 5). This is similar to the neuroarchitecture in *Drosophila*, in location and appearance (Ito et al., 2014). In contrast, locusts and bees have two BUs, the medial and lateral BU (Träger et al., 2008; Pfeiffer and Kinoshita, 2012; Zeller et al., 2015; Held et al., 2016; Mota et al., 2016). Another small but separate neuropil presented in the dung beetle LX is the gall (GA). This neuropil has also been described in *Drosophila* (Ito et al., 2014; Wolff et al., 2015) where it receives output connections from the CBL (Ito et al., 2013; Wolff et al., 2015). This seems to coincide with the bifurcated fiber tract that runs between the GA and central body (CB) in dung beetles (*CBGT*; Fig. 5). In the monarch butterfly, the same neuropil has been termed the anterior loblet (Heinze and Reppert, 2012) and also receives input specifically from the CBL via columnar neurons (Heinze et al., 2013). The functional role of the GA, however, is still unknown. The rest of the LX in dung beetles is composed of the lateral accessory lobe (LAL), which has been described in its detailed extent only in a limited number of species. This is possibly due to its ambiguous boundaries. Although the functional role of the LAL is still unclear, a number of studies suggest that it serves as a premotor center and as an output site for the CX (reviewed by Namiki and Kanzaki, 2016). The LAL also participates in the late processing stage of polarized light signals, downstream of the CX (Heinze and Homberg, 2009; Heinze and Reppert, 2011). A common characteristic of the LAL across species is its immunoreactivity to anti-5-HT, which stains an extensive network of fiber branches that delineate the LAL boundaries (Iwano et al., 2010; Heinze and Reppert, 2012; Namiki and Kanzaki, 2016). The anti-5-HT immunoreactivity was present, albeit faint (possibly due to poor antisera penetration), also in dung beetles. The dung beetle LAL was characterized also by another feature that seems to be conserved across

holo- and hemimetabolous species: the presence of two subunit, the upper LAL and the lower LAL (Heinze and Homberg, 2008; el Jundi et al., 2010; Iwano et al., 2010; Heinze and Reppert, 2012; Ito et al., 2014; Bressan et al., 2015; Namiki and Kanzaki, 2016). Whether this separation has any functional relevance, as suggested by Namiki and Kanzaki (2016), is still unclear.

Central complex

As in many insects, such as locusts (Homberg et al., 2011; Homberg, 2015) and monarch butterflies (Heinze and Reppert, 2011), the internal celestial compass of dung beetles most probably lies in the central complex (CX; el Jundi et al., 2015b). Due to its central role in integration of multisensory information, however, the CX would be expected to also participate in other tasks (for a review see Pfeiffer and Homberg, 2014). The dung beetle CX consists of three unpaired neuropils (the protocerebral bridge (PB), the lower division of the central body (CBL), and the upper division of the central body (CBU)) and one paired neuropil (the noduli (NO); Fig. 6). These neuropils are arranged in a similar fashion as in other insects, especially, in the monarch butterfly (Heinze and Reppert, 2012): the PB lies posterior to the CBU, which is closely neighbored by the CBL on the anterior side, and by the paired NO that lie beneath it (Fig. 6).

The PB, CBU, and CBL are characterized by a varying number of vertical slices in other insects (Heinze and Homberg, 2008; Heinze et al., 2013; Wolff et al., 2015), and in the case of CBL and CBU, also by intersecting horizontal layers (Heinze and Homberg, 2008; Heinze and Reppert, 2012; Heinze et al., 2013; Wolff et al., 2015). In locusts and monarch butterflies, the CBL has been shown to consist of at least five and four horizontal layers, respectively (Müller et al., 1997; Heinze et al., 2013) and relays celestial compass information from the BU into the CX (Homberg et al., 2011; el Jundi et al., 2015b). The dung beetle CBL however, could not be divided into layers by means of anti-synapsin staining (as in the case of the CBU, Fig. 6A3,A4,B3,B4). However, previously described TL neurons in *S. lamarcki* (el Jundi et al., 2015b) indicate that the CBL is layered also in dung beetles. Moreover, the dung beetle CBL appears to have an organized structure, as evidenced by evenly distributed bright vertical slices in the anti-synapsin staining (Fig. 6C1). In dung beetles, the CL1 and CPU1 columnar neurons innervate slice-like regions in the CBL and CBU (el Jundi et al., 2015b), respectively. This corresponds with the innervation pattern of columnar neurons in the CB of other species (Homberg et al., 2011; Heinze et al., 2013) and suggests that the dung beetle's CB also consists of highly organized horizontal layers and vertical slices.

In locusts and monarch butterflies, the CBU is organized into 8 slices (Heinze and Homberg, 2008; Homberg et al., 2011; Heinze et al., 2013). In the fan-shaped body of the *Drosophila*, which is equivalent to the CBU, the sliced organization seems to be looser as their numbers vary among the nine horizontal layers (Wolff et al., 2015). The number of reported horizontal layers in other species is lower. The locust CBU consists of overall five layers (three main layers with two layers further divided into two sublayers; Heinze and Homberg, 2008), whereas the monarch butterfly CBU is consisted of at least six layers (four main layers with layers II and III subdivided into two additional layers; Heinze and Reppert, 2012). The CBUs in both dung beetles were found to consist of four layers with no sublayers (Fig. 6D). Although these layers show some similarity with those present in the locust, it is difficult to assess the homology between these species without connectivity maps of individual neurons. Such mapping might also result in a higher number of layers not visible with immunohistochemistry. Reciprocally, layer characterizations provide a useful reference frame to study mapping of single neuron connectivity.

Instead of being divided as in moths and butterflies (el Jundi et al., 2009; Heinze and Reppert, 2012), the layout of the dung beetle PB is continuous, sharing similarity in appearance with the one described in most insects, including *Drosophila* (Ito et al., 2014), the red flour

beetle (Dreyer et al., 2010), and the ant *Cardiocondyla obscurior* (Bressan et al., 2015). The PB in dung beetles consists of 16 slices distributed evenly on both sides of the brain midline. This organization is commonly found in the PB of other species, and has been shown to form the basis for a neuronal map of the 360° azimuthal space of polarized skylight at least in locusts (Heinze and Homberg, 2007).

Antennal lobe

The antennal lobe (AL) in *S. lamarcki* and *S. satyrus* were found to consist of about 83 and 86 glomeruli, respectively. However, as the glomeruli become more difficult to define towards posterior, we cannot exclude the possibility that these values vary between individual animals of the same species. This number of glomeruli falls within the range of 60-90 glomeruli reported in other Coleopteran species, such as the red flour beetle *Tribolium castaneum*, the small hive beetle *Aethina tumida* or the scarab beetle *Holotrichia diomphalia* (Dreyer et al., 2010; Hu et al., 2011; Dippel et al., 2016; Kollmann et al., 2016). Since the courtship behavior of *S. lamarcki* involves sexual pheromones secreted by the male beetle (Burger, 2014), at least subtle dimorphism within the olfactory system would be expected, but we did not find any sex-specific glomeruli in dung beetles. This is similar to the situation in *T. castaneum* and *A. tumida* (Dreyer et al., 2010; Kollmann et al., 2016), but different to the AL of *H. diomphalia* that includes a group of glomeruli that are sexual dimorphic and encode pheromones (Hu et al., 2011). Further studies are required to find out how pheromones are processed in the dung beetle brain and if such differences are present in the AL.

An interesting similarity between the dung beetle and the red flour beetle ALs is the presence of a glomerulus that clearly stands out from the rest of the AL glomeruli by both appearance and its slightly separated location in the ventromedial corner of the AL (AGL in Fig. 7; Dippel et al., 2016). A similar region, termed *lobus glomerulatus*, has also been found in the brain of the cockroach *Periplaneta americana*, where it is more separated from the AL and has been assigned to the tritocerebrum and is considered to be involved in the processing of gustatory information (Ernst et al., 1977; Wei et al., 2010). In the red flour beetle, the corresponding neuropil exclusively receives input from the mouthparts (palps) and also serves a gustatory function (Dippel et al., 2016). A “special” glomerulus that does not receive input from the ANs has also been described in moths (Kent et al., 1986; el Jundi et al., 2009) and mosquitos (Distler and Boeckh, 1997). In these insects however, this distinct glomerulus responds to the presence of CO_2 and is innervated by sensory fibers that originate from the labial palps in moths and maxillary palps in mosquitos (Stange, 1992; Grant et al., 1995; Guerenstein et al., 2004). The AGL in dung beetles seems to be also devoid of any connections to the sensory fibers projecting from the antennae, and it is thus plausible that this glomerulus receives olfactory/gustatory information from the mouthparts also in these insects (Fig. 7C). However, since our observation is based on two antennal backfills, it is not clear yet whether the AGL should be assigned to the deutocerebral AL (and receives input from the AL) or whether it is truly homologous to the orthopteran *lobus glomerulatus* and thus part of the tritocerebrum.

We found altogether four *ALT* projecting from the ALH in the core of the dung beetle ALs. The profile of these tracts is very similar to those described in the moth *Heliothis virescens* (Ian et al., 2016a) with the exception of the *lALT* having thinner appearance in dung beetles (Fig. 9C). The profile is also similar to that in *Drosophila*, except for the more medial position of the *lALT* in dung beetles (Fig. 9C; Tanaka et al., 2012a; b). As in other species, the *mALT* was found to be the thickest *ALT*, and could be clearly distinguished from the rest by a strongly anti-5-HT-immunoreactive fiber. Presumably, this fiber belongs to a 5-HT-immunoreactive neuron that is found across species and innervates most, if not all of the AL glomeruli and runs through the *mALT* into the CA (Schachtner et al., 2005; Dacks et al., 2006;

Kloppenburg and Mercer, 2008). As in the noctuid moth *Heliothis virescens*, the *mALT* in dung beetles seems to be the only *ALT* that directly connects the AL and the mushroom body calyx (CA) (Fig 9D-F; Ian et al., 2016). While the *mlALT* in dung beetles seems to connect specifically to the lateral horn (LH), the *tALT* bifurcates and appears to make connections also to the protocerebrum. These connection patterns are similar to those in *Drosophila* (Tanaka et al., 2012b) and *Heliothis* (Ian et al., 2016a; b).

Mushroom body

The structural complexity and architecture of the mushroom body (MB) varies across species, often reflecting the sensory and behavioral ecology of an insect (Strausfeld et al., 2009; Farris, 2015, 2016). Perhaps the clearest indications of interspecies variation can be observed in the architecture to the CA: some species possess an elaborate and multi-compartmented CA while in others it can be either minuscule or completely lacking (Strausfeld et al., 2009). A well-studied example of a large and complex CA is provided by the honey bee. Their calyx is bi-parted, each part consisting of three domains (the lip, the collar, and the basal ring) and each of these three domains receives different sensory inputs (Ehmer and Gronenberg, 2002). While the lip is innervated primarily by olfactory neurons (Schröter and Malun, 2000; Abel et al., 2001; Gronenberg, 2001), the collar receives information primarily from optic lobe neurons (Gronenberg, 1986, 2001; Ehmer and Gronenberg, 2002; Paulk and Gronenberg, 2008). Similarly, in butterflies (*Papilio xuthus*), moths (*Daphnia elpenor* and *Macroglossum stellatarum*) and the fruit fly, the CA is multi-compartmented and receives olfactory information to the primary CA, while visual inputs specifically innervate the accessory CA or also the inner zones within the primary CA (Tanaka et al., 2008; Kinoshita et al., 2015; Stöckl et al., 2016a; Vogt et al., 2016).

The CA in dung beetles seem to lack an accessory calyx and we were not able to find any evidence for visual inputs into the CA. Our data thus suggest that the dung beetle CA rather receives mainly olfactory information. This type of singular structure is typical for specialized dung-feeding beetles, and stands in contrast to the divided and more complex CAs found in generalist beetles (Farris and Roberts, 2005).

The remaining parts of the dung beetle MBs, i.e. the pedunculus (PED), and the MB lobes and their sublobes, are very similar to those described in the red flour beetle (Fig 8.; Zhao et al., 2008; Heuer et al., 2012; Binzer et al., 2014). Except for the lack of a spur, the dung beetle MBs share great similarity also with the *Drosophila* MBs (Tanaka et al., 2008). The dung beetles MBs also lack satellite structures, such the Y tract and the associated Y lobe found among *Lepidoptera* (Pearson, 1971; Homberg et al., 1988; Sjöholm et al., 2005; Heinze and Reppert, 2012; Montgomery and Ott, 2015; Montgomery et al., 2016).

An interesting additional finding however, was the presence of fibers connecting the αL,α'L and the lateral horn (*αLHT* ; Fig. 9D-F). These fibers are reminiscent of the extrinsic α lobe neuron fibers found in *Drosophila* (Ito et al., 1998). These include the MB-V2 neurons, responsible for the retrieval of aversive olfactory memories (Séjourné et al., 2011). Whether the *αLHT* found in dung beetles consists of fibers of similar origin remains to be seen in future investigations.

Central adjoining neuropils

Due to their rather contiguous appearance and a lack of clear boundaries, the central adjoining neuropils (CANP) have been described in only three species so far, the monarch butterfly(Heinze and Reppert, 2012), the ant *Cardiocondyla obscurior* (Bressan et al., 2015), and *Drosophila* (Ito et al., 2014). In accordance with previous studies, the dung beetle CANP were delineated with the help of fiber-bundle landmarks (Fig. 9; see also Table 2). Most of the bundles found corresponded to those described previously, while the some could not be directly

related to possible counterparts in other species. These bundles included the *iPLPC*, *MOC*, *IOT*, *CTT*, *SLPT*, *lSMPT*, and *CBGT* (associated with the lateral complex) were named according to their association to given neuropils or to fibers projecting from the optic lobe (as in the case of *MOC* and *IOT*).

Except for the separated gnathal ganglia (GNG), the layout and the relative sizes of the CANP groups in the dung beetle brain are very similar to those in the fruit fly and monarch butterfly (despite the labeling difference in the latter) (Fig. 10-11; see also supplementary movie 1; Heinze and Reppert, 2012; Ito et al., 2014). What functional relevance these similarities might reflect is a difficult question as very little is known about what type of information these neuropils process. Nevertheless, although species-specific allometric differences do occur (see below), the CANP seem to have a relatively high degree of homology across species.

In the dung beetle and *Drosophila*, the superior neuropils (SNP) and ventrolateral neuropils (VLNP) are relatively large, laterally flanked by another prominent neuropil, the lateral horn (LH). The LH is considered to be a part of the olfactory system, but may process multimodal information (Strausfeld et al., 2007; Ruta et al., 2010; Gupta and Stopfer, 2012). These neuropils are large also in the monarch butterfly, although the presence of a neuropil analogous to the SIP was not reported (Heinze and Reppert, 2012). In contrast, in ants, the SNP are much smaller in relative size with the typically closely neighboring LH and optic tubercles undetectable without tracer injections (Bressan et al., 2015). Bressan et al. (2015) suggested that this relative size difference might correlate with the small size of the ant optic lobe.

The ventrolateral protocerebrum (VLP) and the posterior lateral protocerebrum (PLP), which belong to the VLNP along with the AOTU (and wedge in *Drosophila*; (Ito et al., 2014)), appear to primarily process visual information (Otsuna and Ito, 2006; Strausfeld and Okamura, 2007; Strausfeld et al., 2007; Mu et al., 2012). The VLP and PLP are prominent in all four species. With respect to the rest of the CANP groups the similarities are less obvious. While the inferior neuropils (INP) and the ventromedial neuropils (VMNP) are similar in dung beetles, monarch butterflies and *Drosophila*, they appear to be different in the ant *Cardiocondyla obscurior*. This mismatch most likely results from differences in the way these neuropils' boundaries were defined, and whether certain neuropils, e.g. the inferior protocerebrum in the ant brain, have been further divided into subunits or not (Heinze and Reppert, 2012; Ito et al., 2014; Bressan et al., 2015). In addition, the enormous volume of the mushroom bodies in ants might affect the relative sizes of surrounding neuropils, including the VMNP, thus, resulting in differences. The subesophageal neuropils in the monarch and the ant (including the GNG; Heinze and Reppert, 2012; Bressan et al., 2015), and the corresponding periesophageal neuropils (PENP) in the dung beetle (excluding the GNG; Fig. 11) are described as a single structure, while in *Drosophila* it has been divided into at least five different neuropils, including the AMMC (and excluding the GNG; Ito et al., 2014). We were not able to further subdivide it into neuropils as the unfused brain (the cerebrum is connected to the GNG via long circumesophageal connectives) possibly leads to a differently shaped tritocerebrum and, thus, makes it difficult to find the homologous regions of the *Drosophila* PENP in the beetle brain. Shedding more light into interspecies differences or homologies with regards to the CANP would require neuronal mapping and developmental studies (Ito et al., 2013; Yu et al., 2013).

Taken together, even though we found a few differences between the dung beetle brain and the brain of other insects, the general layout is remarkably similar between different insect orders and many brain regions could be characterized also in the beetle brain. Not only describing the areas of the cerebrum that are relatively easy to define, but also the CANP, is a key to further understand which brain areas are interconnected in the insect brain and how these neuropils interact to use and translate information into a relevant behavior.

ACKNOWLEDGEMENTS

The authors would like to thank the following people: Keram Pfeiffer, Wolf Huetteroth, and Gavin Taylor for fruitful discussions regarding nomenclature and data interpretation; Johanna Chavez for helping with neuropil reconstructions; Erich Buchner and Christian Wegener for providing the anti-synapsin antibody; Adrian Bell for proofreading the manuscript; and Jochen Smolka for providing the photograph of *S. lamarcki*. This project was funded by Knut and Alice Wallenberg foundation and the Swedish Research Council.

CONFLICT OF INTEREST STATEMENT

The authors declare no conflict of interest.

ROLE OF AUTHORS

Study design: EVI, MD, BeJ. Preparation and acquisition of data: EVI, BeJ. Analysis of data EVI, BeJ. Interpretation of data: EVI, SH, BeJ. Drafting of the manuscript: EVI. Critical review of the manuscript: MD, SH, BeJ. All authors approved on the final version of the manuscript.

DATA ACCESSIBILITY

3D reconstructions of the brain neuropils of *S. lamarcki* are available at the Insect Brain Database website (Species Identification Number: SIN-00006; https://www.insectbraindb.org/species/6/). A movie showing the grey image stack of the dung beetle's central brain (*S. lamarcki*) with labelled neuropils can be found on the journal webpage as a supplementary movie.

LITERATURE CITED

Abel R, Rybak J, Menzel R. 2001. Structure and response patterns of olfactory interneurons in the honeybee, *Apis mellifera*. J Comp Neurol 437:363–83.

Aso Y, Hattori D, Yu Y, Johnston RM, Iyer NA, Ngo T-T, Dionne H, Abbott L, Axel R, Tanimoto H, Rubin GM. 2014a. The neuronal architecture of the mushroom body provides a logic for associative learning. Elife 3:e04577.

Aso Y, Sitaraman D, Ichinose T, Kaun KR, Vogt K, Belliart-Guérin G, Plaçais P-Y, Robie AA, Yamagata N, Schnaitmann C, Rowell WJ, Johnston RM, Ngo T-TB, Chen N, Korff W, Nitabach MN, Heberlein U, Preat T, Branson KM, Tanimoto H, Rubin GM. 2014b. Mushroom body output neurons encode valence and guide memory-based action selection in *Drosophila*. Elife 3:e04580.

Baird E, Byrne MJ, Smolka J, Warrant EJ, Dacke M. 2012. The dung beetle dance: an orientation behaviour? PLoS One 7:e30211.

Bender JA, Pollack AJ, Ritzmann RE. 2010. Neural activity in the central complex of the insect brain is linked to locomotor changes. Curr Biol 20:921–6.

Binzer M, Heuer CM, Kollmann M, Kahnt J, Hauser F, Grimmelikhuijzen CJP, Schachtner J. 2014. Neuropeptidome of *Tribolium castaneum* antennal lobes and mushroom bodies. J Comp Neurol 522:337–57.

Blum M, Labhart T. 2000. Photoreceptor visual fields, ommatidial array, and receptor axon projections in the polarisation-sensitive dorsal rim area of the cricket compound eye. J Comp Physiol A 186:119–28.

Brandt R, Rohlfing T, Rybak J, Krofczik S, Maye A, Westerhoff M, Hege H-C, Menzel R. 2005. Three-dimensional average-shape atlas of the honeybee brain and its applications. J Comp Neurol 492:1–19.

Bressan JMA, Benz M, Oettler J, Heinze J, Hartenstein V, Sprecher SG. 2015. A map of brain neuropils and fiber systems in the ant *Cardiocondyla obscurior*. Front Neuroanat 8:166.

Bräunig P, Burrows M. 2004. Projection patterns of posterior dorsal unpaired median neurons of the locust subesophageal ganglion. J Comp Neurol 478:164–75.

Burger BBV. 2014. First investigation of the semiochemistry of South African dung beetle species. In: Mucignat-Caretta C, editor. Neurobiology of chemical communication. CRC Press/Taylor & Francis. p 57–98.

Byrne M, Dacke M. 2011. The visual ecology of dung beetles. In: Simmons LW, Ridshill-Smith TJ, editors. Ecology and evolution of dung beetles. John Wiley & Sons, Inc. p 177–199.

Byrne M, Dacke M, Nordström P, Scholtz C, Warrant E. 2003. Visual cues used by ball-rolling dung beetles for orientation. J Comp Physiol A Neuroethol Sens Neural Behav Physiol 189:411–8.

Chiang A-S, Lin C-Y, Chuang C-C, Chang H-M, Hsieh C-H, Yeh C-W, Shih C-T, Wu J-J, Wang G-T, Chen Y-C, Wu C-C, Chen G-Y, Ching Y-T, Lee P-C, Lin C-Y, Lin H-H, Wu C-C, Hsu H-W, Huang Y-A, Chen J-Y, Chiang H-J, Lu C-F, Ni R-F, Yeh C-Y, Hwang J-K. 2011. Three-dimensional reconstruction of brain-wide wiring networks in *Drosophila* at single-cell resolution. Curr Biol 21:1–11.

Cohn R, Morantte I, Ruta V. 2015. Coordinated and compartmentalized neuromodulation shapes sensory processing in *Drosophila*. Cell 163:1742–55.

Dacke M, Baird E, Byrne M, Scholtz CH, Warrant EJ. 2013a. Dung beetles use the Milky Way for orientation. Curr Biol 23:298–300.

Dacke M, Byrne M, Smolka J, Warrant E, Baird E. 2013b. Dung beetles ignore landmarks for straight-line orientation. J Comp Physiol A Neuroethol Sens Neural Behav Physiol 199:17–23.

Dacke M, Byrne MJ, Baird E, Scholtz CH, Warrant EJ. 2011. How dim is dim? Precision of the celestial compass in moonlight and sunlight. Philos Trans R Soc Lond B Biol Sci 366:697–702.

Dacke M, Byrne MJ, Scholtz CH, Warrant EJ. 2004. Lunar orientation in a beetle. Proceedings Biol Sci 271:361–5.

Dacke M, el Jundi B, Smolka J, Byrne M, Baird E. 2014. The role of the sun in the celestial compass of dung beetles. Philos Trans R Soc Lond B Biol Sci 369:20130036.

Dacke M, Nilsson D-E, Scholtz CH, Byrne M, Warrant EJ. 2003a. Animal behaviour: insect orientation to polarized moonlight. Nature 424:33.

Dacke M, Nordström P, Scholtz CH. 2003b. Twilight orientation to polarised light in the crepuscular dung beetle *Scarabaeus zambesianus*. J Exp Biol 206:1535–43.

Dacks AM, Christensen TA, Hildebrand JG. 2006. Phylogeny of a serotonin-immunoreactive neuron in the primary olfactory center of the insect brain. J Comp Neurol 498:727–46.

Dippel S, Kollmann M, Oberhofer G, Montino A, Knoll C, Krala M, Rexer K-H, Frank S, Kumpf R, Schachtner J, Wimmer EA. 2016. Morphological and transcriptomic analysis of a beetle chemosensory system reveals a gnathal olfactory center. BMC Biol 14:90.

Distler, Boeckh. 1997. Central projections of the maxillary and antennal nerves in the mosquito *Aedes aegypti*. J Exp Biol 200:1873–9.

Dormont L, Jay-Robert P, Bessière J-M, Rapior S, Lumaret J-P. 2010. Innate olfactory preferences in dung beetles. J Exp Biol 213:3177–86.
Dreyer D, Vitt H, Dippel S, Goetz B, el Jundi B, Kollmann M, Huetteroth W, Schachtner J. 2010. 3D standard brain of the red flour beetle *Tribolium castaneum*: a tool to study metamorphic development and adult plasticity. Front Syst Neurosci 4:3.
Ehmer B, Gronenberg W. 2002. Segregation of visual input to the mushroom bodies in the honeybee (*Apis mellifera*). J Comp Neurol 451:362–73.
el Jundi B, Foster JJ, Byrne MJ, Baird E, Dacke M. 2015a. Spectral information as an orientation cue in dung beetles. Biol Lett 11:20150656.
el Jundi B, Foster JJ, Khaldy L, Byrne MJ, Dacke M, Baird E. 2016. A snapshot-based mechanism for celestial orientation. Curr Biol 26:1456–62.
el Jundi B, Heinze S, Lenschow C, Kurylas A, Rohlfing T, Homberg U. 2010. The locust standard brain: a 3D standard of the central complex as a platform for neural network analysis. Front Syst Neurosci 3:21.
el Jundi B, Huetteroth W, Kurylas AE, Schachtner J. 2009. Anisometric brain dimorphism revisited: Implementation of a volumetric 3D standard brain in *Manduca sexta*. J Comp Neurol 517:210–25.
el Jundi B, Pfeiffer K, Heinze S, Homberg U. 2014a. Integration of polarization and chromatic cues in the insect sky compass. J Comp Physiol A Neuroethol Sens Neural Behav Physiol 200:575–89.
el Jundi B, Pfeiffer K, Homberg U. 2011. A distinct layer of the medulla integrates sky compass signals in the brain of an insect. PLoS One 6:e27855.
el Jundi B, Smolka J, Baird E, Byrne MJ, Dacke M. 2014b. Diurnal dung beetles use the intensity gradient and the polarization pattern of the sky for orientation. J Exp Biol 217:2422–9.
el Jundi B, Warrant EJ, Byrne MJ, Khaldy L, Baird E, Smolka J, Dacke M. 2015b. Neural coding underlying the cue preference for celestial orientation. Proc Natl Acad Sci U S A 112:11395–400.
Ernst KD, Boeckh J, Boeckh V. 1977. A neuroanatomical study on the organization of the central antennal pathways in insects. Cell Tissue Res 176:285–306.
Fabian-Fine R, Volknandt W, Seyfarth E. 1999. Peripheral synapses at identifiable mechanosensory neurons in the spider *Cupiennius salei*: synapsin-like immunoreactivity. Cell Tissue Res 295:13–9.
Farris SM. 2015. Evolution of brain elaboration. Philos Trans R Soc Lond B Biol Sci 370.
Farris SM. 2016. Insect societies and the social brain. Curr Opin insect Sci 15:1–8.
Farris SM, Roberts NS. 2005. Coevolution of generalist feeding ecologies and gyrencephalic mushroom bodies in insects. Proc Natl Acad Sci U S A 102:17394–9.
Forgie SA, Kryger U, Bloomer P, Scholtz CH. 2006. Evolutionary relationships among the Scarabaeini (Coleoptera: Scarabaeidae) based on combined molecular and morphological data. Mol Phylogenet Evol 40:662–78.
Fortini ME, Rubin GM. 1991. The optic lobe projection pattern of polarization-sensitive photoreceptor cells in *Drosophila melanogaster*. Cell Tissue Res 265:185–91.
Godenschwege TA, Reisch D, Diegelmann S, Eberle K, Funk N, Heisenberg M, Hoppe V, Hoppe J, Klagges BRE, Martin J-R, Nikitina EA, Putz G, Reifegerste R, Reisch N, Rister J, Schaupp M, Scholz H, Schwärzel M, Werner U, Zars TD, Buchner S, Buchner E. 2004. Flies lacking all synapsins are unexpectedly healthy but are impaired in complex behaviour. Eur J Neurosci 20:611–22.
Grant AJ, Aghajanian JG, O'Connell RJ, Wigton BE. 1995. Electrophysiological responses of receptor neurons in mosquito maxillary palp sensilla to carbon dioxide. J Comp Physiol A 177:389–396.

Greiner B, Ribi WA, Wcislo WT, Warrant EJ. 2004. Neural organisation in the first optic ganglion of the nocturnal bee *Megalopta genalis*. Cell Tissue Res 318:429–37.
Gronenberg W. 1986. Physiological and anatomical properties of optical input-fibres to the mushroom body in the bee brain. J Insect Physiol 32:695–704.
Gronenberg W. 2001. Subdivisions of hymenopteran mushroom body calyces by their afferent supply. J Comp Neurol 435:474–89.
Gronenberg W, Hölldobler B. 1999. Morphologic representation of visual and antennal information in the ant brain. J Comp Neurol 412:229–40.
Guerenstein PG, Christensen TA, Hildebrand JG. 2004. Sensory processing of ambient CO2 information in the brain of the moth *Manduca sexta*. J Comp Physiol A Neuroethol Sens Neural Behav Physiol 190:707–25.
Guo P, Ritzmann RE. 2013. Neural activity in the central complex of the cockroach brain is linked to turning behaviors. J Exp Biol 216:992–1002.
Gupta N, Stopfer M. 2012. Functional analysis of a higher olfactory center, the lateral horn. J Neurosci 32:8138–48.
Hansson BS, Stensmyr MC. 2011. Evolution of insect olfaction. Neuron 72:698–711.
Harzsch S, Benton J, Dawirs RR, Beltz B. 1999. A new look at embryonic development of the visual system in decapod crustaceans: neuropil formation, neurogenesis, and apoptotic cell death. J Neurobiol 39:294–306.
Heinze S, Florman J, Asokaraj S, el Jundi B, Reppert SM. 2013. Anatomical basis of sun compass navigation II: the neuronal composition of the central complex of the monarch butterfly. J Comp Neurol 521:267–98.
Heinze S, Homberg U. 2007. Maplike representation of celestial E-vector orientations in the brain of an insect. Science 315:995–7.
Heinze S, Homberg U. 2008. Neuroarchitecture of the central complex of the desert locust: Intrinsic and columnar neurons. J Comp Neurol 511:454–78.
Heinze S, Homberg U. 2009. Linking the input to the output: new sets of neurons complement the polarization vision network in the locust central complex. J Neurosci 29:4911–21.
Heinze S, Reppert SM. 2011. Sun compass integration of skylight cues in migratory monarch butterflies. Neuron 69:345–58.
Heinze S, Reppert SM. 2012. Anatomical basis of sun compass navigation I: the general layout of the monarch butterfly brain. J Comp Neurol 520:1599–628.
Heisenberg M. 2003. Mushroom body memoir: from maps to models. Nat Rev Neurosci 4:266–75.
Heisenberg M, Borst A, Wagner S, Byers D. 1985. *Drosophila* mushroom body mutants are deficient in olfactory learning. J Neurogenet 2:1–30.
Held M, Berz A, Hensgen R, Muenz TS, Scholl C, Rössler W, Homberg U, Pfeiffer K. 2016. Microglomerular synaptic complexes in the sky-compass network of the honeybee connect parallel pathways from the anterior optic tubercle to the central complex. Front Behav Neurosci 10:186.
Helfrich-Förster C. 2004. Neurobiology of the fruit fly's circadian clock. Genes, Brain Behav 4:65–76.
Heuer CM, Kollmann M, Binzer M, Schachtner J. 2012. Neuropeptides in insect mushroom bodies. Arthropod Struct Dev 41:199–226.
Hige T, Aso Y, Rubin GM, Turner GC. 2015. Plasticity-driven individualization of olfactory coding in mushroom body output neurons. Nature 526:258–62.
Homberg U. 2008. Evolution of the central complex in the arthropod brain with respect to the visual system. Arthropod Struct Dev 37:347–62.
Homberg U. 2015. Sky compass orientation in desert locusts - evidence from field and

laboratory studies. Front Behav Neurosci 9:346.
Homberg U, Heinze S, Pfeiffer K, Kinoshita M, el Jundi B. 2011. Central neural coding of sky polarization in insects. Philos Trans R Soc Lond B Biol Sci 366:680–7.
Homberg U, Hofer S, Pfeiffer K, Gebhardt S. 2003a. Organization and neural connections of the anterior optic tubercle in the brain of the locust, *Schistocerca gregaria*. J Comp Neurol 462:415–30.
Homberg U, Montague RA, Hildebrand JG. 1988. Anatomy of antenno-cerebral pathways in the brain of the sphinx moth *Manduca sexta*. Cell Tissue Res 254:255–281.
Homberg U, Paech A. 2002. Ultrastructure and orientation of ommatidia in the dorsal rim area of the locust compound eye. Arthropod Struct Dev 30:271–80.
Homberg U, Reischig T, Stengl M. 2003b. Neural organization of the circadian system of the cockroach *Leucophaea maderae*. Chronobiol Int 20:577–91.
Hu J-H, Wang Z-Y, Sun F. 2011. Anatomical organization of antennal-lobe glomeruli in males and females of the scarab beetle *Holotrichia diomphalia* (Coleoptera: Melonthidae). Arthropod Struct Dev 40:420–8.
Ian E, Berg A, Lillevoll SC, Berg BG. 2016a. Antennal-lobe tracts in the noctuid moth, *Heliothis virescens*: new anatomical findings. Cell Tissue Res 366.
Ian E, Zhao XC, Lande A, Berg BG. 2016b. Individual neurons confined to distinct antennal-lobe tracts in the Heliothine moth: Morphological characteristics and global projection patterns. Front Neuroanat 10:101.
Ito K, Shinomiya K, Ito M, Armstrong JD, Boyan G, Hartenstein V, Harzsch S, Heisenberg M, Homberg U, Jenett A, Keshishian H, Restifo LL, Rössler W, Simpson JH, Strausfeld NJ, Strauss R, Vosshall LB, Insect Brain Name Working Group. 2014. A systematic nomenclature for the insect brain. Neuron 81:755–65.
Ito K, Suzuki K, Estes P, Ramaswami M, Yamamoto D, Strausfeld NJ. 1998. The organization of extrinsic neurons and their implications in the functional roles of the mushroom bodies in *Drosophila melanogaster* Meigen. Learn Mem 5:52–77.
Ito M, Masuda N, Shinomiya K, Endo K, Ito K. 2013. Systematic analysis of neural projections reveals clonal composition of the *Drosophila* brain. Curr Biol 23:644–55.
Iwano M, Hill ES, Mori A, Mishima T, Mishima T, Ito K, Kanzaki R. 2010. Neurons associated with the flip-flop activity in the lateral accessory lobe and ventral protocerebrum of the silkworm moth brain. J Comp Neurol 518:366–88.
Jenett A, Rubin GM, Ngo T-TB, Shepherd D, Murphy C, Dionne H, Pfeiffer BD, Cavallaro A, Hall D, Jeter J, Iyer N, Fetter D, Hausenfluck JH, Peng H, Trautman ET, Svirskas RR, Myers EW, Iwinski ZR, Aso Y, DePasquale GM, Enos A, Hulamm P, Lam SCB, Li H-H, Laverty TR, Long F, Qu L, Murphy SD, Rokicki K, Safford T, Shaw K, Simpson JH, Sowell A, Tae S, Yu Y, Zugates CT. 2012. A GAL4-driver line resource for *Drosophila* neurobiology. Cell Rep 2:991–1001.
Kent KS, Harrow ID, Quartararo P, Hildebrand JG. 1986. An accessory olfactory pathway in Lepidoptera: the labial pit organ and its central projections in *Manduca sexta* and certain other sphinx moths and silk moths. Cell Tissue Res 245:237–45.
Kinoshita M, Shimohigasshi M, Tominaga Y, Arikawa K, Homberg U. 2015. Topographically distinct visual and olfactory inputs to the mushroom body in the Swallowtail butterfly, *Papilio xuthus*. J Comp Neurol 523:162–82.
Klagges BR, Heimbeck G, Godenschwege TA, Hofbauer A, Pflugfelder GO, Reifegerste R, Reisch D, Schaupp M, Buchner S, Buchner E. 1996. Invertebrate synapsins: a single gene codes for several isoforms in *Drosophila*. J Neurosci 16:3154–65.
Kloppenburg P, Mercer AR. 2008. Serotonin modulation of moth central olfactory neurons. Annu Rev Entomol 53:179–90.
Kollmann M, Rupenthal AL, Neumann P, Huetteroth W, Schachtner J. 2016. Novel antennal

lobe substructures revealed in the small hive beetle *Aethina tumida*. Cell Tissue Res 363:679–692.
Kurylas AE, Rohlfing T, Krofczik S, Jenett A, Homberg U. 2008. Standardized atlas of the brain of the desert locust, *Schistocerca gregaria*. Cell Tissue Res 333:125–45.
Labhart T, Meyer EP. 1999. Detectors for polarized skylight in insects: a survey of ommatidial specializations in the dorsal rim area of the compound eye. Microsc Res Tech 47:368–79.
Lin C, Strausfeld NJ. 2012. Visual inputs to the mushroom body calyces of the whirligig beetle *Dineutus sublineatus*: modality switching in an insect. J Comp Neurol 520:2562–74.
Mansourian S, Corcoran J, Enjin A, Löfstedt C, Dacke M, Stensmyr MC. 2016. Fecal-derived phenol induces egg-laying aversion in *Drosophila*. Curr Biol 26:2762–2769.
Mappes M, Homberg U. 2004. Behavioral analysis of polarization vision in tethered flying locusts. J Comp Physiol A Neuroethol Sens Neural Behav Physiol 190:61–8.
Martin JP, Guo P, Mu L, Harley CM, Ritzmann RE. 2015. Central-complex control of movement in the freely walking cockroach. Curr Biol 25:2795–803.
Menzel R. 2014. The insect mushroom body, an experience-dependent recoding device. J Physiol Paris 108:84–95.
Midgley JJ, White JDM, Johnson SD, Bronner GN. 2015. Faecal mimicry by seeds ensures dispersal by dung beetles. Nat Plants 1:15141.
Montgomery SH, Merrill RM, Ott SR. 2016. Brain composition in *Heliconius* butterflies, posteclosion growth and experience-dependent neuropil plasticity. J Comp Neurol 524:1747–69.
Montgomery SH, Ott SR. 2015. Brain composition in *Godyris zavaleta*, a diurnal butterfly, Reflects an increased reliance on olfactory information. J Comp Neurol 523:869–91.
Mota T, Gronenberg W, Giurfa M, Sandoz J-C. 2013. Chromatic processing in the anterior optic tubercle of the honey bee brain. J Neurosci 33:4–16.
Mota T, Kreissl S, Carrasco Durán A, Lefer D, Galizia G, Giurfa M. 2016. Synaptic organization of microglomerular clusters in the lateral and medial bulbs of the honeybee brain. Front Neuroanat 10:103.
Mota T, Yamagata N, Giurfa M, Gronenberg W, Sandoz J-C. 2011. Neural organization and visual processing in the anterior optic tubercle of the honeybee brain. J Neurosci 31:11443–56.
Mu L, Ito K, Bacon JP, Strausfeld NJ. 2012. Optic glomeruli and their inputs in *Drosophila* share an organizational ground pattern with the antennal lobes. J Neurosci 32:6061–71.
Müller M, Homberg U, Kühn A. 1997. Neuroarchitecture of the lower division of the central body in the brain of the locust (*Schistocerca gregaria*). Cell Tissue Res 288:159–76.
Namiki S, Kanzaki R. 2016. Comparative neuroanatomy of the lateral accessory lobe in the insect brain. Front Physiol 7:244.
Ofstad TA, Zuker CS, Reiser MB. 2011. Visual place learning in *Drosophila melanogaster*. Nature 474:204–207.
Otsuna H, Ito K. 2006. Systematic analysis of the visual projection neurons of *Drosophila melanogaster*. I. Lobula-specific pathways. J Comp Neurol 497:928–58.
Ott SR. 2008. Confocal microscopy in large insect brains: zinc-formaldehyde fixation improves synapsin immunostaining and preservation of morphology in whole-mounts. J Neurosci Methods 172:220–30.
Paulk AC, Gronenberg W. 2008. Higher order visual input to the mushroom bodies in the bee, *Bombus impatiens*. Arthropod Struct Dev 37:443–58.
Pearson L. 1971. The corpora pedunculata of *Sphinx ligustri* L. and other Lepidoptera: an anatomical study. Philos Trans R Soc London B Biol Sci 259:477–516.

Pfeiffer K, Homberg U. 2014. Organization and functional roles of the central complex in the insect brain. Annu Rev Entomol 59:165–84.
Pfeiffer K, Kinoshita M. 2012. Segregation of visual inputs from different regions of the compound eye in two parallel pathways through the anterior optic tubercle of the bumblebee (*Bombus ignitus*). J Comp Neurol 520:212–29.
Pfeiffer K, Kinoshita M, Homberg U. 2005. Polarization-sensitive and light-sensitive neurons in two parallel pathways passing through the anterior optic tubercle in the locust brain. J Neurophysiol 94:3903–15.
Phillips-Portillo J, Strausfeld NJ. 2012. Representation of the brain's superior protocerebrum of the flesh fly, *Neobellieria bullata*, in the central body. J Comp Neurol 520:3070–87.
Rein K, Zöckler M, Mader MT, Grübel C, Heisenberg M. 2002. The *Drosophila* standard brain. Curr Biol 12:227–31.
Reischig T, Stengl M. 2003. Ectopic transplantation of the accessory medulla restores circadian locomotor rhythms in arrhythmic cockroaches (*Leucophaea maderae*). J Exp Biol 206:1877–86.
Rospars JP, Hildebrand JG. 2000. Sexually dimorphic and isomorphic glomeruli in the antennal lobes of the sphinx moth *Manduca sexta*. Chem Senses 25:119–29.
Ruta V, Datta SR, Vasconcelos ML, Freeland J, Looger LL, Axel R. 2010. A dimorphic pheromone circuit in *Drosophila* from sensory input to descending output. Nature 468:686–90.
Schachtner J, Schmidt M, Homberg U. 2005. Organization and evolutionary trends of primary olfactory brain centers in Tetraconata (Crustacea+Hexapoda). Arthropod Struct Dev 34:257–299.
Schmeling F, Tegtmeier J, Kinoshita M, Homberg U. 2015. Photoreceptor projections and receptive fields in the dorsal rim area and main retina of the locust eye. J Comp Physiol A Neuroethol Sens Neural Behav Physiol 201:427–40.
Schmitt F, Stieb SM, Wehner R, Rössler W. 2016. Experience-related reorganization of giant synapses in the lateral complex: Potential role in plasticity of the sky-compass pathway in the desert ant *Cataglyphis fortis*. Dev Neurobiol 76:390–404.
Schröter U, Malun D. 2000. Formation of antennal lobe and mushroom body neuropils during metamorphosis in the honeybee, *Apis mellifera*. J Comp Neurol 422:229–245.
Seelig JD, Jayaraman V. 2013. Feature detection and orientation tuning in the *Drosophila* central complex. Nature 503:262–6.
Seelig JD, Jayaraman V. 2015. Neural dynamics for landmark orientation and angular path integration. Nature 521:186–91.
Séjourné J, Plaçais P-Y, Aso Y, Siwanowicz I, Trannoy S, Thoma V, Tedjakumala SR, Rubin GM, Tchénio P, Ito K, Isabel G, Tanimoto H, Preat T. 2011. Mushroom body efferent neurons responsible for aversive olfactory memory retrieval in *Drosophila*. Nat Neurosci 14:903–10.
Sjöholm M, Sinakevitch I, Ignell R, Strausfeld NJ, Hansson BS. 2005. Organization of Kenyon cells in subdivisions of the mushroom bodies of a lepidopteran insect. J Comp Neurol 491:290–304.
Stange G. 1992. High resolution measurement of atmospheric carbon dioxide concentration changes by the labial palp organ of the moth *Heliothis armigera* (Lepidoptera: Noctuidae). J Comp Physiol A 171:317–324.
Strausfeld NJ. 1976. Atlas of an insect brain. (Strausfeld NJ, editor.). Berlin, Heidelberg: Springer Berlin Heidelberg.
Strausfeld NJ. 2012. Arthropod Brains. (Strausfeld NJ, editor.). Harvard University Press.
Strausfeld NJ, Okamura J-Y. 2007. Visual system of calliphorid flies: organization of optic glomeruli and their lobula complex efferents. J Comp Neurol 500:166–88.

Strausfeld NJ, Sinakevitch I, Brown SM, Farris SM. 2009. Ground plan of the insect mushroom body: functional and evolutionary implications. J Comp Neurol 513:265–91.
Strausfeld NJ, Sinakevitch I, Okamura J-Y. 2007. Organization of local interneurons in optic glomeruli of the dipterous visual system and comparisons with the antennal lobes. Dev Neurobiol 67:1267–88.
Stöckl A, Heinze S, Charalabidis A, el Jundi B, Warrant E, Kelber A. 2016a. Differential investment in visual and olfactory brain areas reflects behavioural choices in hawk moths. Sci Rep 6:26041.
Stöckl AL, Heinze S. 2015. A clearer view of the insect brain-combining bleaching with standard whole-mount immunocytochemistry allows confocal imaging of pigment-covered brain areas for 3D reconstruction. Front Neuroanat 9:121.
Stöckl AL, Ribi WA, Warrant EJ. 2016b. Adaptations for nocturnal and diurnal vision in the hawkmoth lamina. J Comp Neurol 524:160–75.
Tanaka NK, Endo K, Ito K. 2012a. Organization of antennal lobe-associated neurons in adult *Drosophila melanogaster* brain. J Comp Neurol 520:4067–130.
Tanaka NK, Suzuki E, Dye L, Ejima A, Stopfer M. 2012b. Dye fills reveal additional olfactory tracts in the protocerebrum of wild-type *Drosophila*. J Comp Neurol 520:4131–40.
Tanaka NK, Tanimoto H, Ito K. 2008. Neuronal assemblies of the *Drosophila* mushroom body. J Comp Neurol 508:711–55.
Tride GD, Burger BBV. 2011. Olfactory ecology. In: Simmons LW, Ridshill-Smith TJ, editors. Ecology and evolution of dung beetles. John Wiley & Sons, Inc. p 87–106.
Träger U, Wagner R, Bausenwein B, Homberg U. 2008. A novel type of microglomerular synaptic complex in the polarization vision pathway of the locust brain. J Comp Neurol 506:288–300.
Varga AG, Ritzmann RE. 2016. Cellular basis of head direction and contextual cues in the insect brain. Curr Biol 26:1816–28.
Vogt K, Aso Y, Hige T, Knapek S, Ichinose T, Friedrich AB, Turner GC, Rubin GM, Tanimoto H. 2016. Direct neural pathways convey distinct visual information to *Drosophila* mushroom bodies. Elife 5:e14009.
Warrant E, Dacke M. 2011. Vision and visual navigation in nocturnal insects. Annu Rev Entomol 56:239–54.
Warrant EJ. 2008. Seeing in the dark: vision and visual behaviour in nocturnal bees and wasps. J Exp Biol 211:1737–46.
Webb B, Wystrach A. 2016. Neural mechanisms of insect navigation. Curr Opin insect Sci 15:27–39.
Wei H, el Jundi B, Homberg U, Stengl M. 2010. Implementation of pigment-dispersing factor-immunoreactive neurons in a standardized atlas of the brain of the cockroach *Leucophaea maderae*. J Comp Neurol 518:4113–33.
Weir PT, Dickinson MH. 2015. Functional divisions for visual processing in the central brain of flying *Drosophila*. Proc Natl Acad Sci U S A 112:E5523-32.
Weir PT, Henze MJ, Bleul C, Baumann-Klausener F, Labhart T, Dickinson MH. 2016. Anatomical reconstruction and functional imaging reveal an ordered array of skylight polarization detectors in *Drosophila*. J Neurosci 36:5397–5404.
Weir PT, Schnell B, Dickinson MH. 2014. Central complex neurons exhibit behaviorally gated responses to visual motion in *Drosophila*. J Neurophysiol 111:62–71.
Wernet MF, Velez MM, Clark DA, Baumann-Klausener F, Brown JR, Klovstad M, Labhart T, Clandinin TR. 2012. Genetic dissection reveals two separate retinal substrates for polarization vision in *Drosophila*. Curr Biol 22:12–20.
Williams JLD. 1975. Anatomical studies of the insect central nervous system: A ground-plan

of the midbrain and an introduction to the central complex in the locust, Schistocerca gregaria (Orthoptera). J Zool 176:67–86.
Wolff T, Iyer NA, Rubin GM. 2015. Neuroarchitecture and neuroanatomy of the *Drosophila* central complex: A GAL4-based dissection of protocerebral bridge neurons and circuits. J Comp Neurol 523:997–1037.
Yu H-H, Awasaki T, Schroeder MD, Long F, Yang JS, He Y, Ding P, Kao J-C, Wu GY-Y, Peng H, Myers G, Lee T. 2013. Clonal development and organization of the adult *Drosophila* central brain. Curr Biol 23:633–43.
Zeller M, Held M, Bender J, Berz A, Heinloth T, Hellfritz T, Pfeiffer K. 2015. Transmedulla neurons in the sky compass network of the honeybee (*Apis mellifera*) are a possible site of circadian input. PLoS One 10:e0143244.
Zhao X, Coptis V, Farris SM. 2008. Metamorphosis and adult development of the mushroom bodies of the red flour beetle, *Tribolium castaneum*. Dev Neurobiol 68:1487–502.

RESOURCES CITED

FIJI: http://fiji.sc; RRID: SCR_002285; Amira 5.3.3: http://www.amiravis.com; RRID: SCR_007353.

FIGURE LEGENDS

Figure 1. The South African ball-rolling dung beetle; while rolling a ball and its brain. **A:** The diurnal species, *Scarabaeus lamarcki*, rolling a dung ball in its natural habitat in South Africa (courtesy of Jochen Smolka). **B:** A microphotograph of the dorsal part of the head of *S. lamarcki* after the removal of the dorsal head capsule and tissues above the brain. The cerebrum (CR), the optic stalks (OS) and the dorsal compound eyes (DE) are visible. **C:** A microphotography of a dissected *S. lamarcki* brain, showing CR, OS, ventral retina (VR), dorsal retina (DR), optic lobe (OL), circumesophageal connectives (CEC), gnathal ganglia (GNG), and the first and second thoracic ganglia (TG). d: dorsal; m: medial; l: lateral; v: ventral. Scale bar in C = 1 mm.

Figure 2. General overview of the diurnal (*S. lamarcki;* D) and nocturnal (*S. satyrus;* N) dung beetle brain hemispheres. **A-C:** Anterior (A), posterior (B) and dorsal (C1) views of three-dimensional (3D) reconstructed and texture-based volume rendered right and left hemispheres of a diurnal and nocturnal dung beetle brain, respectively. The well-defined major neuropils, including dorsal lamina (DLA), ventral lamina (VLA), medulla (ME), accessory medulla (AME), lobula (LO), lobula plate (LOP), antennal lobe (AL), anterior optic tubercle (AOTU), central body (CB), noduli (NO), protocerebral bridge (PB), mushroom body (MB), and gnathal ganglia (GNG) are shown. The mushroom body lobes can be divided into ventral (VL) and medial lobe (ML), as well as pedunculus (PED). The remaining cerebrum (RC) is reconstructed as a single transparent structure shown in grey. C2: the same as C1 but without brain surface. **D-E:** Major midbrain neuropils of the diurnal (D) and nocturnal (E) beetle from oblique medial views. **F:** Optical slices through the diurnal (left) and nocturnal (right) brains from anterior (F1) to posterior (F5) stained against synapsin. The approximate slice depths from the anterior surface: (F1): D = 96 µm, N = 60 µm; (F2): D = 170 µm, N = 240 µm; (F3): D = 202 µm, N = 240 µm; (F4): D = 242 µm, N = 313 µm; (F5): D = 372 µm, N = 397 µm. d: dorsal; m: medial; l: lateral; v: ventral. Scale bars: A-C, F = 1 mm; D-E = 500 µm.

Figure 3. Anatomy of the neuropils in the optic lobe. **A-B:** 3D reconstructions and texture-based volume renderings of the major optic lobe neuropils in the diurnal (A) and nocturnal (B) beetle brain viewed from anterior (A1,B1), posterior (A2,B2), ventral (A3,B3), and oblique dorsomedial (A4,B4). In the nocturnal species a specialized area of the dorsal lamina, most likely the dorsal rim area (LADRA) was found. In both species, the medulla and lobula can be divided into outer (OME) and inner medulla (IME), and outer (OLO) and inner lobula (ILO), respectively. Note the prominent first optic chiasms (*OCH1*) between LA and ME. **C-D:** Frontal optical slices (anti-synapsin immunoreactivity) through the optic lobes (C, diurnal; D, nocturnal) progressing from anterior (C1,D1) to posterior (C3,D3). Note the notch in the lamina in the nocturnal species (arrowhead) separating the LADRA and DLA in the nocturnal beetle. The arrow indicates the region where the medulla can be divided into a ventral and dorsal medulla. The serpentine layer (SPL) separates the OME and IME. The insets in subpanels C3 and D3 show horizontal optical sections of the dorsal lobula plate (LOP). Slice depths (from the anterior OL surface): (C1,D1): D = 40 µm, N = 46 µm; (C2,D2): D = 140 µm, N = 102 µm; (C3,D3): D = 238 µm, N = 188 µm. **E-J:** Maximum intensity projections of frontal optical sections through the DLA (E, diurnal; F, nocturnal), the dorsal medulla (G, diurnal; I, nocturnal), and ventral medulla (H, diurnal; J, nocturnal) based on (subpanels 1) anti-synapsin, and (subpanels 2) anti-5-HT-staining. Subpanels 3 show the merges of the anti-synapsin (magenta) and anti-serotonin (green) stainings. Number of layers are indicated by numbers and the boundaries by solid lines. a: anterior; p: posterior; d: dorsal; m: medial; l: lateral; v: ventral. Scale bars: A-B = 200 µm; C-J = 100 µm.

Figure 4. The anterior optic tubercle in the beetle brain. **A:** Tracer injections into the dorsal medulla reveal fibers projecting from the dorsal medulla via the anterior optic tract (*AOT*) into the AOTU (A1) in the diurnal dung beetle brain. A2-A3 show maximum intensity projections (A2: normal; A3: inverted) of the AOTU highlighted in (A1), showing the lower unit complex (LUC) consisting of six subunits (I-VI), and the upper unit (UU). A4 shows the 3D surface reconstruction of the AOTU (in A2-A3) and its compartments from anterior view. **B-C:** Frontal optical slices of anti-synapsin-labelled AOTU in the diurnal (B) and nocturnal (C) beetle from anterior (B1,C1) to posterior (B3,C3), showing all divisions. In subpanels C2 and D2, *AOT* originating from the ipsilateral optic lobe is also visible. **D-E:** 3D reconstructions of the AOTU in the diurnal (D) and nocturnal (E) beetle brain shown from anterior (D1,E1), dorsal (D2,E2) and oblique ventroposterior (D3,E3). a: anterior; p: posterior; d: dorsal; m: medial; l: lateral; v: ventral. Scale bars: A1 = 500 µm; A2-A4 = 100 µm; B-E = 100 µm.

Figure 5. Anatomy of the lateral complex. **A:** Frontal optical slices through the lateral complex (diurnal species, right hemisphere) at different depths from anterior (A1) to posterior (A4). The approximate depths measured from the anterior edge of the lateral complex: A1 = 30 µm; A2 = 75 µm; A3 = 90 µm; A4 = 133 µm. The dotted lines indicate the boundaries of the neuropils, which include the lateral accessory lobe (LAL), consisting of the upper (ULAL) and lower (LLAL) division, the bulb (BU), and the gall (GA), consisting of three subunits; ventral gall (VGA), dorsal gall (DGA) and gall tip (GAT). The insets are cropped versions of the corresponding 5-HT-staining (inverted). Note the brightly stained medial antennal lobe tract (*mALT*) and the isthmus tract (*IT*). **B-E:** Surface reconstructions of the lateral complex neuropils (B,C) and fiber bundles (D,E) in the diurnal (B,D) and nocturnal (C,E) brain shown from anterior (subpanels 1), posterior (subpanels 2), oblique dorsolateral (subpanels 3), and dorsal (subpanels 3). The LAL commissure (*LALC*) was used to define the boundaries between ULAL and LLAL. The medial boundary of LAL was defined by *mALT*, while the dorsal boundary of the ULAL was defined by the mushroom bodies, *IT*, the tubercle-to-bulb tract

(*TUBUT*), the bifurcated central-body-to-gall tract (*CBGT*), and the inferior fiber system (*IFS*). a: anterior; p: posterior; d: dorsal; m: medial; l: lateral; v: ventral. Scale bars = 100 µm.

Figure 6. The dung beetle's central complex. **A-B:** 3D models of the central-complex neuropils in the diurnal (A) and nocturnal (B) beetle brain. Anterior (A1,B1), posterior (A2,B2), and sagittally cut lateral (A3,B3) and oblique dorsoanterior (A4,B4) views. The central complex in both species consisted of a lower (CBL) and an upper (CBU) division of the central body, paired noduli (NO) and the protocerebral bridge (PB). Two of the neuropils, CBU and NO, could be subdivided into four layers (subpanels 3 and 4). **C-E:** Frontal (C-D) and sagittal (E) view of the (subpanels 1) anti-synapsin- and (subpanels 2) anti-5-HT-stained CBL (C,E), CBU (C-E) and NO (D,E) in the diurnal beetle. Subpanels 3 show anti-synapsin (magenta) and anti-5-HT (green) stainings merged (the same as in subpanels 1 and 2). C: The CBL is characterized by a faint anti-synapsin and anti-5-HT fluorescence signal showing indications of vertical slices. Anti-5-HT staining shows the isthmus tract (*IT*) running into the CBL. D: In the CBU, the four horizontal layers, I-IV, are shown. E**:** The layered structure of the noduli in the diurnal beetle is shown. **F:** Single frontal optical slice showing the PB in the diurnal dung beetle brain. The structure of the PB was clearly discontinuous and could be divided into 16 slices (slice boundaries indicated by arrows). a: anterior; p: posterior; d: dorsal; v: ventral. Scale bars: A-D & F = 100 µm; E = 50 µm.

Figure 7. The antennal lobes in the dung beetle brain. **A-C:** Backfill of the antennal nerve (*AN*) stains the antennal mechanosensory and motor center (AMMC; A,B) and the antennal lobe (C). **A:** Intensity-dependent 3D rendering of the Neurobiotin staining from oblique ventromedial view showing *AN* and AMMC. **B:** Volume rendering and surface reconstructions of the AMMC superimposed, viewed from anterior. **C:** Maximum intensity projection of antennal-lobe (AL) glomeruli stained by tracer injection. The dotted line highlights the medial boundary of the AL. **D:** Anterior view (intensity-dependent volume rendering) of the AL in the male diurnal beetle brain (anti-synapsin). The accessory glomerulus (AGL) has been indicated. **E:** 3D reconstruction of the antennal lobe from different orientations (the same as in C), starting from anterior and progressing in 90° rotations. The AL glomeruli are color-coded according to ~50 µm intervals in depth from anterior to posterior. The AGL is shown in grey. **F:** Single frontal optical sections of AL at different depths from anterior (F1) to posterior (F5). The approximate locations of the sections are projected onto the medial view of the 3D surface reconstructed AL. The dotted line indicates AGL, while the arrow indicates a fiber bundle penetrating the AGL. ALH is the AL hub. **G-I:** The same as D-F but for the AL of a nocturnal male dung beetle. d: dorsal; m: medial; l: lateral; v: ventral. Scale bars = 200 µm.

Figure 8. Anatomy of the mushroom body. **A-C:** Single frontal optical slices of anti-synapsin- (A), anti-5-HT-stained MB (B), and both stainings overlapped (C) in the diurnal beetle from posterior (subpanels 1) to anterior (subpanels 4). The arrow in panel B indicates the most anterior Kenyon cell bodies. In the same panel arrowheads show two axon bundles originating from two groups of 5-HT-immunoreactive Kenyon cells (subpanel B1 inset) that merge beneath the CA into the pedunculus (PED, see panel B2,C2, and insets in B2,C2). On its anterior side, the PED bifurcates into vertical and medial lobes (VL and ML). VL and ML can be divided into α, α' (αL,α'L), β, β' (βL,β'L), vertical γ (VγL), and γ lobes (MγL). **D-E:** 3D models of the MBs in the diurnal (D) and nocturnal (E) beetle brain shown from anterior (D1,E1), dorsal (D2,E2), and oblique posteromedial (D3,E3). The reconstructions are based on anti-synapsin (transparent) and anti-5-HT (inner lobes) immunoreactivity. a: anterior; p: posterior; d: dorsal; m: medial; l: lateral; v: ventral. Scale bars: A-E and inset in B1 = 100 µm; insets in A2-C2 = 50 µm.

Figure 9. The neuropils and fiber bundles used as landmarks for labelling the central adjoining neuropils. **A-F:** Tracer injections into the antennal lobes (A-C) or calyx (D-F) reveal the antennal lobe tracts, the lateral horn, and the mushroom body lobes. **A:** Anterior view of a 3D intensity-dependent volume rendering shows three of the four antennal lobe tracts, *mALT*, *mlALT* and the transverse antennal lobe tract (*tALT*), all having arborizations in either LH or CA. **B:** Same as in A, but with surface reconstructions of LH and *mALT*. **C:** Oblique posteromedial view of the volume rendering reveals *lALT*, arborizing near the lateral horn (LH). **D:** Intensity-dependent volume rendering of a CA tracer-injection from anterior view. Note the thin αL,α'L-to-LH tract (*αLHT*). **E:** As D, but with surface reconstructions of LH and *mALT* **F**: Oblique medial view of the same reconstruction shown in D and E. **G-J:** The major fiber tracts, commissures, fascicles and fiber systems in the cerebrum (G: anterior view; H: posterior view; I: dorsal view; J: ventral view). The specified neuropils described earlier in this study are shown in transparent grey. Note that only the neuropils from the right hemisphere are shown. a: anterior; p: posterior; d: dorsal; m: medial; l: lateral; v: ventral. Scale bars = 200 µm;

Figure 10. The layout of the central adjoining neuropils in the diurnal dung beetle. **A-D:** Surface reconstructions of the neuropils based on anti-synapsin immunofluorescence (A: anterior view; B: posterior view; C: dorsal view; D: ventral view). Neuropils such as the mushroom bodies, the central complex, the AOTU and the antennal lobes are shown in grey. In the case of bilateral neuropils (e.g. AL), the left neuropils have been omitted for clarity. **E:** Surface reconstruction of GNG (anterior and posterior views) located in the subesophageal region ventrally to the midbrain (see Figs. 1 and 2). **F:** Frontal optical sections (anti-synapsin staining) covering the midbrain from anterior (F1) to posterior (F12). The neuropils are labelled by overlaying with colored, transparent surface cuts taken directly from the 3D reconstructions and by semi-schematic demarcation with dotted lines to enhance clarity. For orientation purposes, the neuropils specified and described earlier are also indicated. The depth of each section was measured from anterior and is shown at the bottom of each panel in yellow. a: anterior; p: posterior; d: dorsal; v: ventral. Scale bars = 200µm.

Figure 11. Surface reconstructions of the central adjoining neuropil groups and associated tracts, fascicles and commissures used as landmarks for defining neuropil boundaries. The left hemispheres have been cut in the sagittal plane to clarify the location of some of the landmarks relative to the neuropils. **A:** Superior neuropils and lateral horn (LH). Important landmarks for defining neuropil boundaries include AOTU, VL, CA, the lateral SMP tract (*lSMPT*), SLP tract (*SLPT*), and the superior fibre system (*SFS*). **B:** Ventrolateral neuropils. The boundaries for the ventrolateral (VLP) and posterior lateral protocerebrum (PLP) were defined using the PED, great commissure (*GC*), the inferior optic tract (*IOT*), lateral equatorial fascicle (*LEF*), the clamp-tritocerebral tract (CTT), and the posterior optic commissure (*POC*). **C:** Inferior neuropils. Boundaries for crepine (CRE), clamp (CL), inferior bridge (IB) and antler (ATL) were defined using *mlALT*, *mALT*, *SFS*, *IOT*, medial equatorial fascicle (*MEF*), *LEF*, *CTT*, *GC*, minor optic commissure (*MOC*), superior PLP commissure (*sPLPC*), ML and PED. The central body has been omitted for clarity. **D:** Ventromedial neuropils. Boundaries for the epaulette (EPA), gorget (GOR), vest (VES) and posterior slope (PS) were determined using *mALT*, *mlALT*, *LEF*, *MEF*, inferior fiber system (*IFS*), inferior PLP commissure (*iPLPC*), *GC* and *POC* as landmarks. **E:** Periesophageal neuropils and antennal mechanosensory and motor center (AMMC). *IFS*, *iPLPC* and *POC* were used to define the superior and posterior boundary of the periesophageal neuropils (PENP). a: anterior; p: posterior; d: dorsal; v: ventral. Scale bars = 200 µm.

TABLE OF ABBREVIATIONS

5-HT	serotonin
AGL	accessory glomerulus
αL,α'L	α, α' lobes
AL	antennal lobe
ALH	antennal lobe hub
αLHT	αL,α'L-to-lateral horn tract
ALT	antennal lobe tract
AME	accessory medulla
AMMC	antennal mechanosensory and motor center
AN	antennal nerve
AOT	anterior optic tract
AOTU	anterior optic tubercle
ATL	antler
βL,β'L	β, β' lobes
BU	bulb
CA	mushroom body calyx
CANP	central adjoining neuropils
CB	central body
CBGT	central body-to-gall tract
CBL	the lower division of the central body
CBU	the upper division of the central body
CEC	circumesophageal connectives
CL	clamp
CR	cerebrum
CRE	crepine
CTT	clamp-tritocerebral tract
CX	central complex
d	dorsal
D	diurnal dung beetle (*S. lamarcki*)
DE	dorsal eye
DGA	dorsal gall
DLA	dorsal lamina
DME	dorsal medulla
DR	dorsal retina
EPA	epaulette
GC	great commissure
GA	gall
GAT	gall tip
GNG	gnathal ganglia
GOR	gorget
IB	inferior bridge
IFS	inferior fiber system
ILO	inner lobula
IME	inner medulla
INP	inferior neuropils
IOT	inferior optic tract
iPLPC	inferior PLP commissure

IT	isthmus tract
l	lateral
LADRA	dorsal rim area of the lamina
LAL	lateral accessory lobe
LALC	lateral accessory lobe commissure
lALT	lateral antennal lobe tract
LEF	lateral equatorial fascicle
LH	lateral horn
LLAL	lower lateral accessory lobe
LO	lobula
lSMPT	lateral superior medial protocerebral tract
LUC	lower unit complex of the anterior optic tubercle
LX	lateral complex
m	medial
mALT	medial antennal lobe tract
MB	mushroom body
ME	medulla
MEF	medial equatorial fascicle
MγL	medial γ lobe
ML	medial lobe
mlALT	mediolateral antennal lobe tract
MOC	minor optic commissure
N	nocturnal dung beetle (*S. satyrus*)
NO	noduli
OCH1	first optic chiasm
OL	optic lobe
OLO	outer lobula
OME	outer medulla
OS	optic stalk
PB	protocerebral bridge
PED	pedunculus
PENP	periesophageal neuropils
PLP	posterior lateral protocerebrum
POC	posterior optic commissure
pPLPC	posterior posterior lateral protocerebral commissure
PS	posterior slope
RC	remaining cerebrum
SFS	superior fiber system
SIP	superior intermediate protocerebrum
SL	serpentine layer
SLP	superior lateral protocerebrum
SLPT	superior lateral protocerebral tract
SMP	superior medial protocerebrum
SNP	superior neuropils
SPL	serpentine layer
sPLPC	superior posterior lateral protocerebral commissure
tALT	transverse antennal lobe tract
TG	thoracic ganglia
TUBUT	tubercle-to-bulb tract
ULAL	upper lateral accessory lobe

UU	upper unit of the anterior optic tubercle
v	ventral
VES	vest
VγL	vertical γ lobe
VL	vertical lobe
VLA	ventral lamina
VLNP	ventrolateral neuropils
VLP	ventrolateral protocerebrum
VME	ventral medulla
VMNP	ventromedial neuropils

TABLES

Table 1. Primary antibodies

Table 2. Comparison of synapse-rich neuropils and landmark fiber bundles between the brains of *Scarabaeus lamarcki* (this work) and *Drosophila melanogaster* (based on Tanaka et al., 2012a; b; Ito et al., 2014; and Wolff et al., 2015). n.d.: not described in *S. lamarcki* or *D. melanogaster*.

Supplementary movie 1. Frontal serial section movie of the *Scarabaeus lamarcki* central brain. The labelled neuropils are also shown.

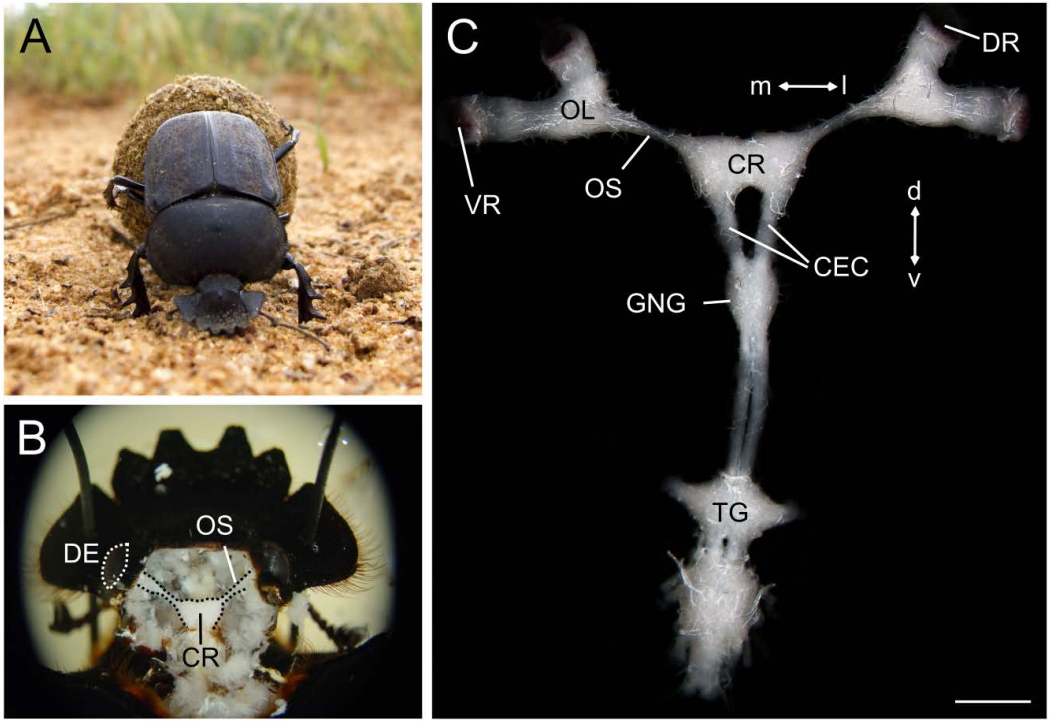
A
B
DE
OS
CR
C
DR
m
l
OL
VR
OS
CR
d
v
CEC
GNG
TG

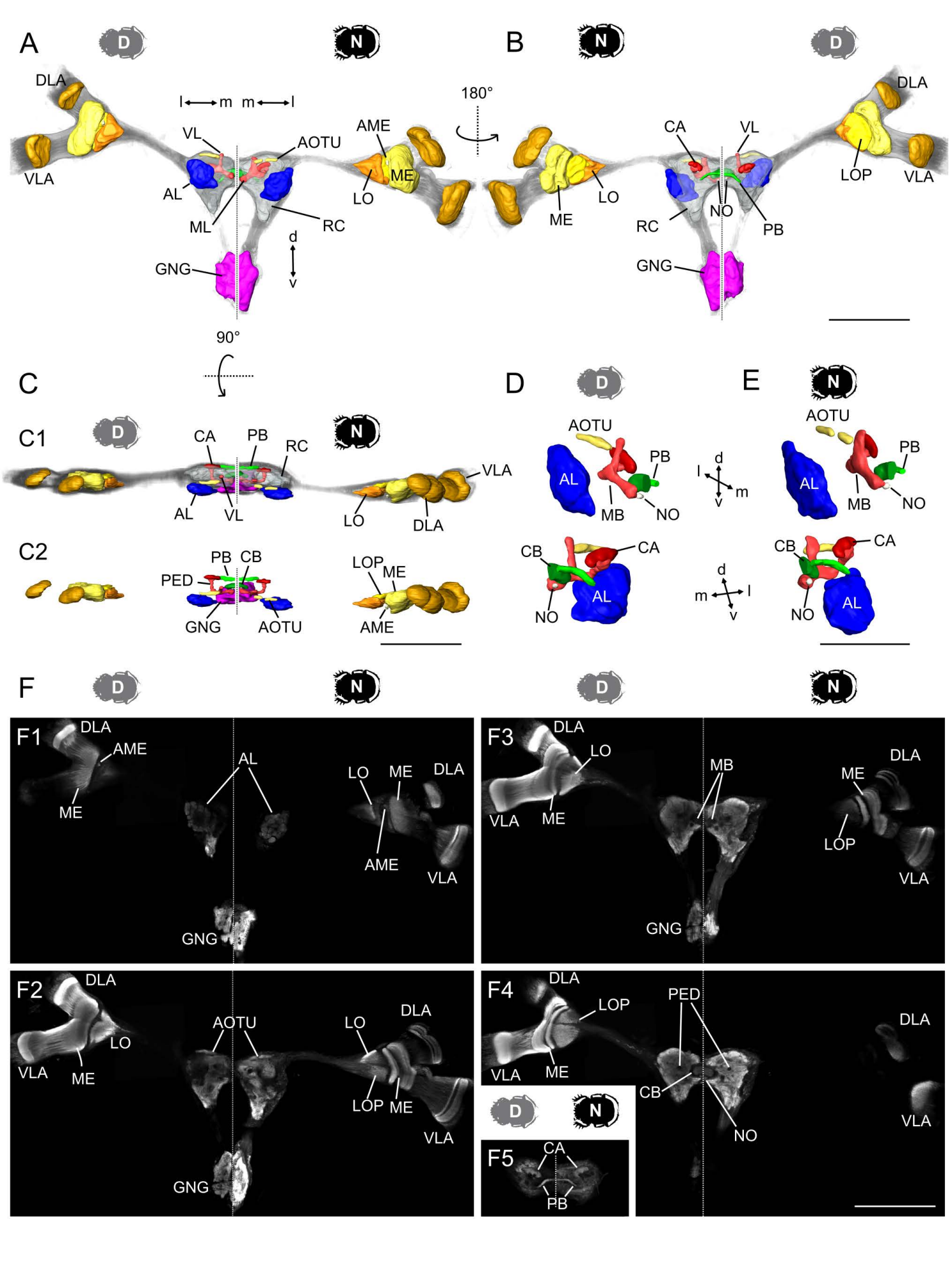
A
D
N
DLA
VLA
l m m l
VL
AOTU
AL
ML
RC
GNG
d
v
AME
ME
LO
180°
B
CA
PB
NO
LOP
90°
C
C1
C2
PED
CB
D
E
F
F1
F2
F3
F4
F5

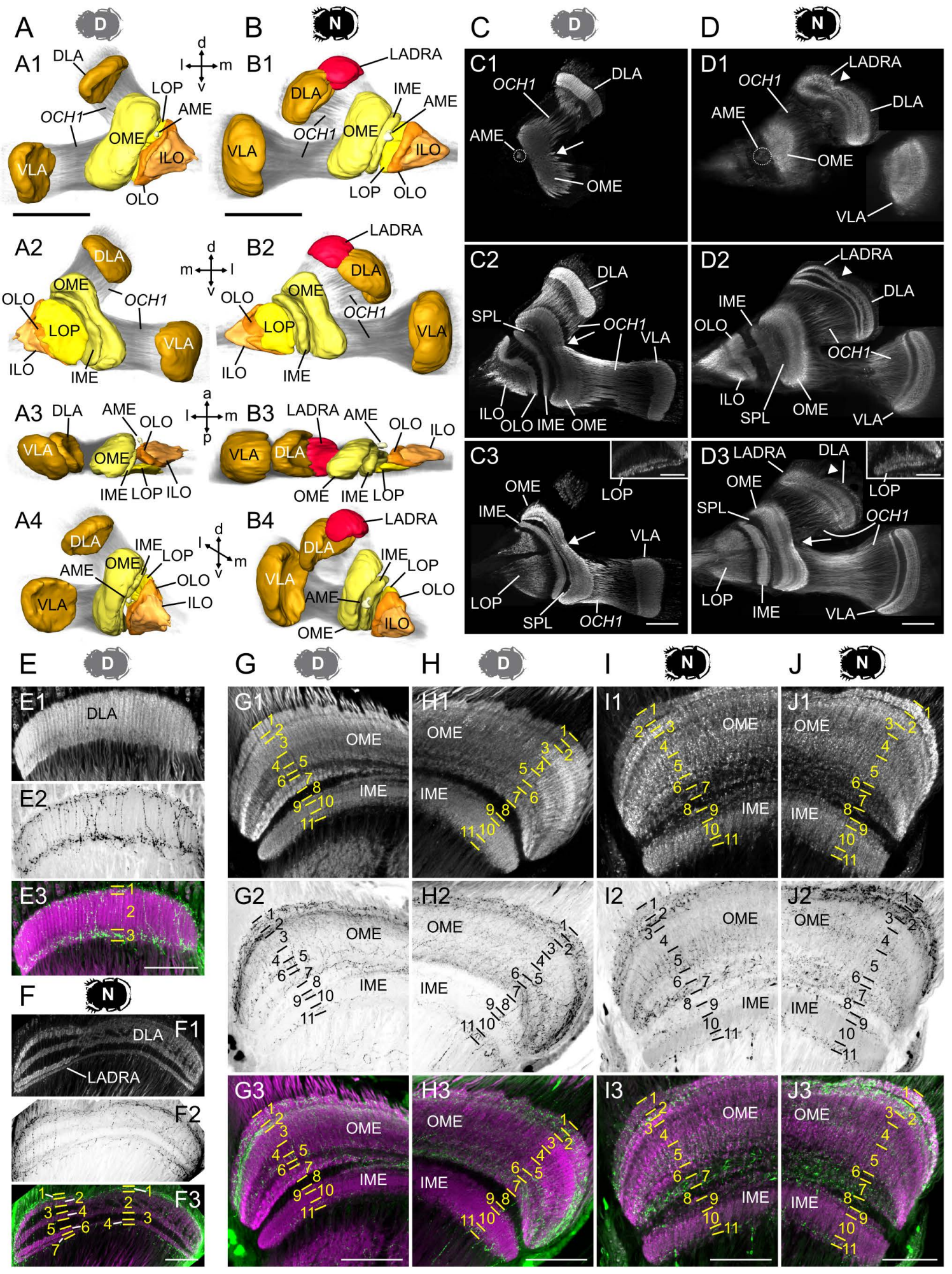
A
D
B
N
C
D
D
N
A1
DLA
LOP
AME
OCH1
OME
ILO
VLA
OLO
d
l
m
v
B1
LADRA
DLA
IME
AME
OCH1
OME
VLA
ILO
LOP
OLO
C1
OCH1
DLA
AME
OME
D1
LADRA
OCH1
DLA
AME
OME
VLA
A2
DLA
OME
OLO
OCH1
LOP
VLA
ILO
IME
B2
LADRA
DLA
OLO
OME
OCH1
LOP
VLA
ILO
IME
C2
DLA
SPL
OCH1
VLA
ILO
OLO
IME
OME
D2
LADRA
DLA
IME
OLO
OCH1
ILO
SPL
OME
VLA
A3
DLA
AME
OLO
VLA
OME
IME
LOP
ILO
a
p
B3
LADRA
AME
OLO
ILO
VLA
DLA
OME
IME
LOP
C3
OME
IME
LOP
VLA
LOP
SPL
OCH1
D3
LADRA
DLA
OME
SPL
OCH1
LOP
LOP
IME
VLA
A4
DLA
IME
LOP
AME
OME
OLO
VLA
ILO
B4
LADRA
DLA
IME
LOP
VLA
AME
OLO
ILO
OME
E
D
G
D
H
D
I
N
J
N
E1
DLA
E2
E3
G1
OME
IME
H1
OME
IME
I1
OME
IME
J1
OME
IME
G2
OME
IME
H2
OME
IME
I2
OME
IME
J2
OME
IME
F
N
F1
DLA
LADRA
F2
F3
G3
OME
IME
H3
OME
IME
I3
OME
IME
J3
OME
IME

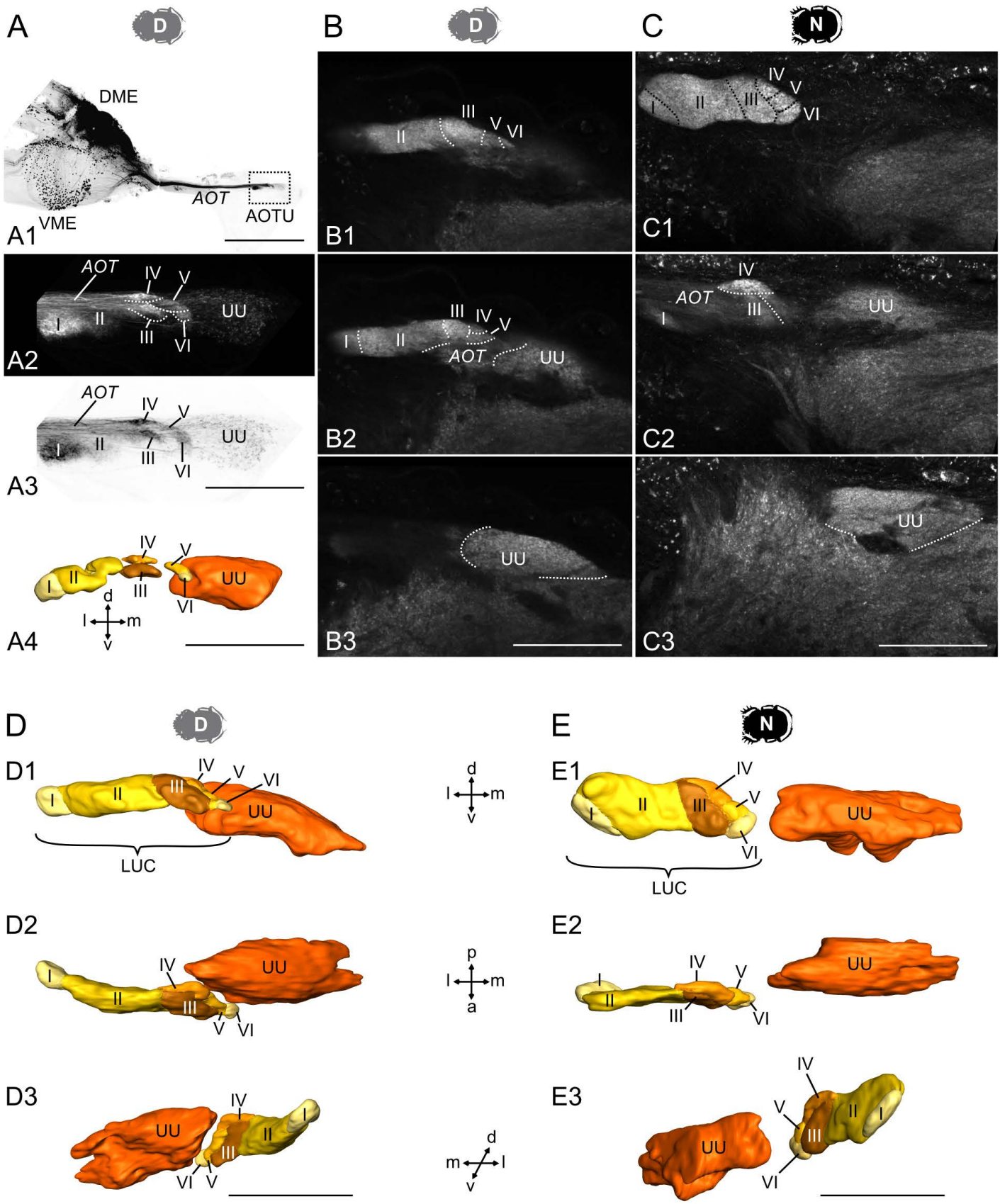
A
D
DME
AOT
AOTU
VME
A1
AOT
IV
V
I
II
III
VI
UU
A2
AOT
IV
V
I
II
III
VI
UU
A3
IV
V
I
II
III
VI
UU
d
l
m
v
A4
B
D
III
V
VI
II
B1
III
IV
V
I
II
AOT
UU
B2
UU
B3
C
N
IV
V
I
II
III
VI
C1
IV
AOT
I
III
UU
C2
UU
C3
D
D
D1
IV
V
VI
I
II
III
UU
LUC
D2
IV
UU
I
II
III
V
VI
D3
IV
UU
I
II
III
VI
V
d
l
m
v
p
l
m
a
E
N
E1
IV
V
I
II
III
VI
UU
LUC
E2
IV
V
UU
I
II
III
VI
E3
IV
V
II
I
III
UU
VI

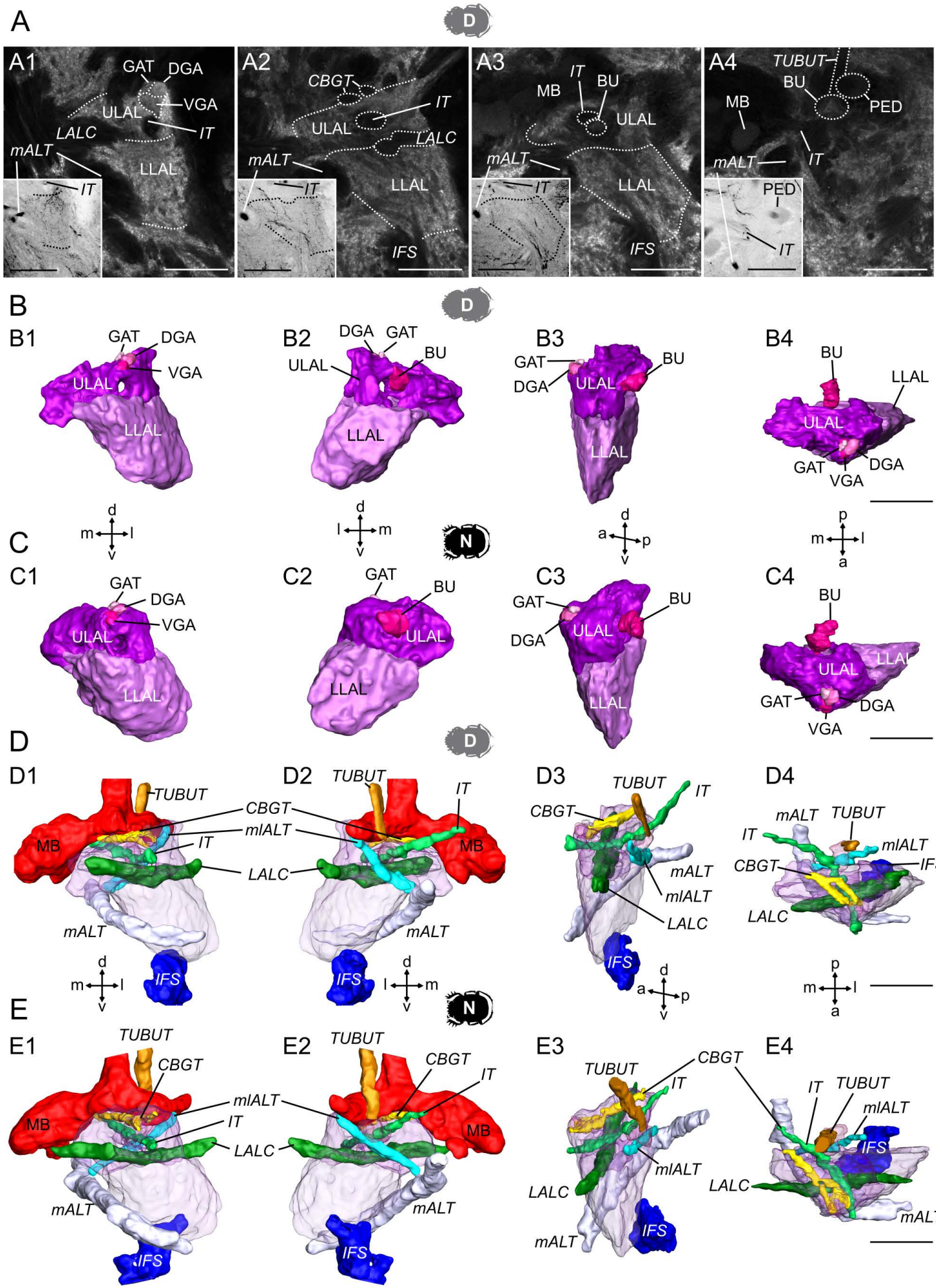
A
D
A1
GAT
DGA
VGA
ULAL
LALC
IT
mALT
LLAL
A2
CBGT
IT
ULAL
LALC
mALT
IT
LLAL
IFS
A3
MB
IT
BU
ULAL
mALT
IT
LLAL
IFS
A4
TUBUT
BU
MB
PED
mALT
IT
PED
IT
B
D
B1
GAT
DGA
VGA
ULAL
LLAL
B2
DGA
GAT
BU
ULAL
LLAL
B3
GAT
DGA
BU
ULAL
LLAL
B4
BU
LLAL
ULAL
GAT
DGA
VGA
C
N
C1
GAT
DGA
VGA
ULAL
LLAL
C2
GAT
BU
ULAL
LLAL
C3
GAT
DGA
BU
ULAL
LLAL
C4
BU
ULAL
LLAL
GAT
DGA
VGA
D
D
D1
TUBUT
CBGT
MB
mlALT
IT
LALC
mALT
IFS
D2
TUBUT
IT
CBGT
MB
mlALT
LALC
mALT
IFS
D3
TUBUT
IT
CBGT
mALT
mlALT
LALC
IFS
D4
mALT
TUBUT
IT
mlALT
CBGT
IFS
LALC
E
N
E1
TUBUT
CBGT
MB
mlALT
IT
LALC
mALT
IFS
E2
TUBUT
CBGT
IT
MB
mALT
IFS
E3
CBGT
TUBUT
IT
mlALT
LALC
mALT
IFS
E4
IT
TUBUT
mlALT
IFS
LALC
mALT

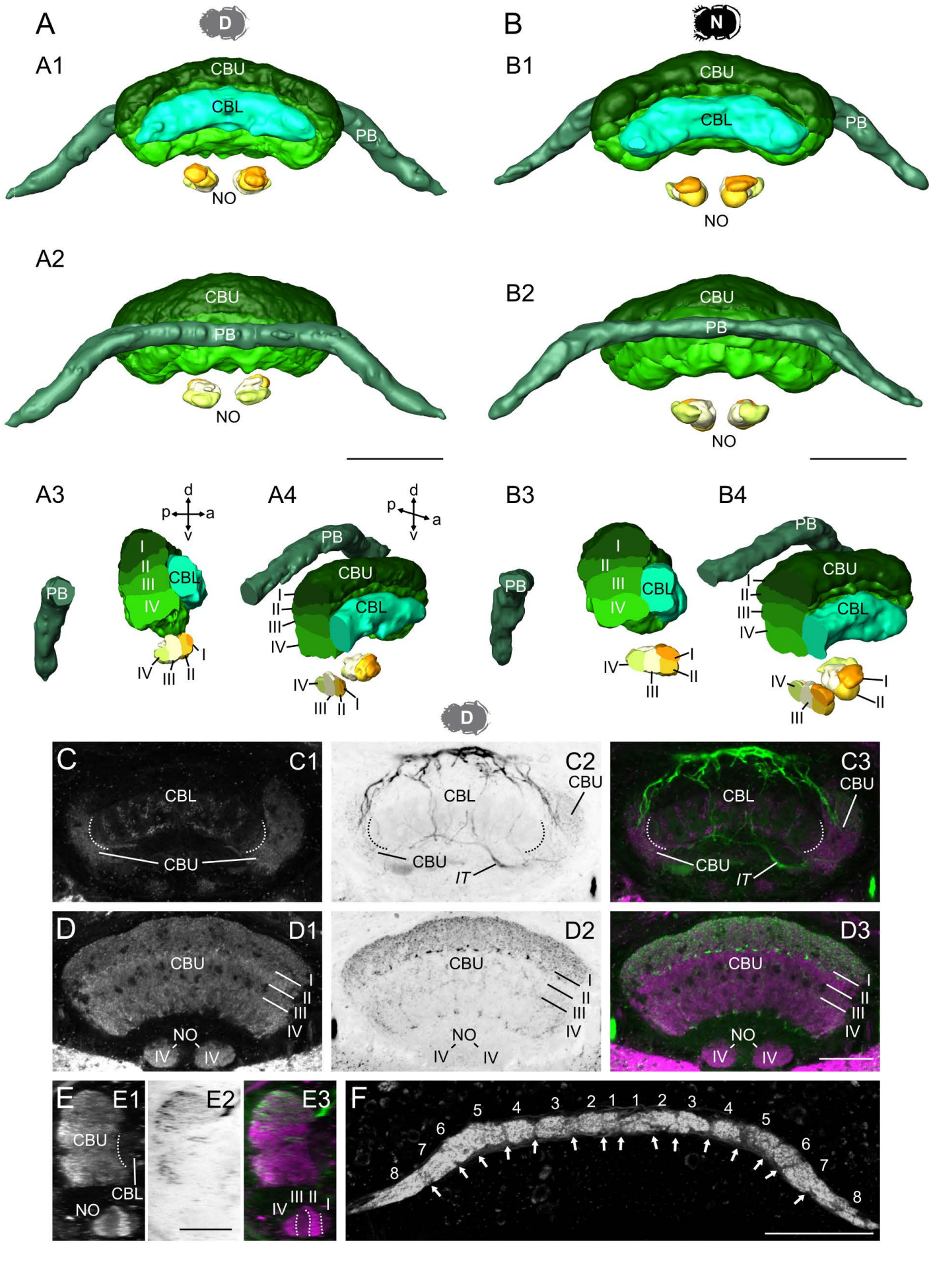
A
D
A1
CBU
CBL
PB
NO
A2
CBU
PB
NO
A3
d
p
a
v
PB
I
II
III
IV
CBL
IV
III
II
I
A4
d
p
a
v
PB
CBU
CBL
I
II
III
IV
IV
III
II
I
B
N
B1
CBU
CBL
PB
NO
B2
CBU
PB
NO
B3
PB
I
II
III
IV
CBL
IV
III
I
II
B4
PB
CBU
CBL
I
II
III
IV
IV
III
I
II
D
C
C1
CBL
CBU
C2
CBU
CBL
CBU
IT
C3
CBU
CBL
CBU
IT
D
D1
CBU
I
II
III
IV
NO
IV
IV
D2
CBU
I
II
III
IV
NO
IV
IV
D3
CBU
I
II
III
IV
NO
IV
IV
E
E1
CBU
CBL
NO
E2
E3
IV
III
II
I
F
1
2
3
4
5
6
7
8

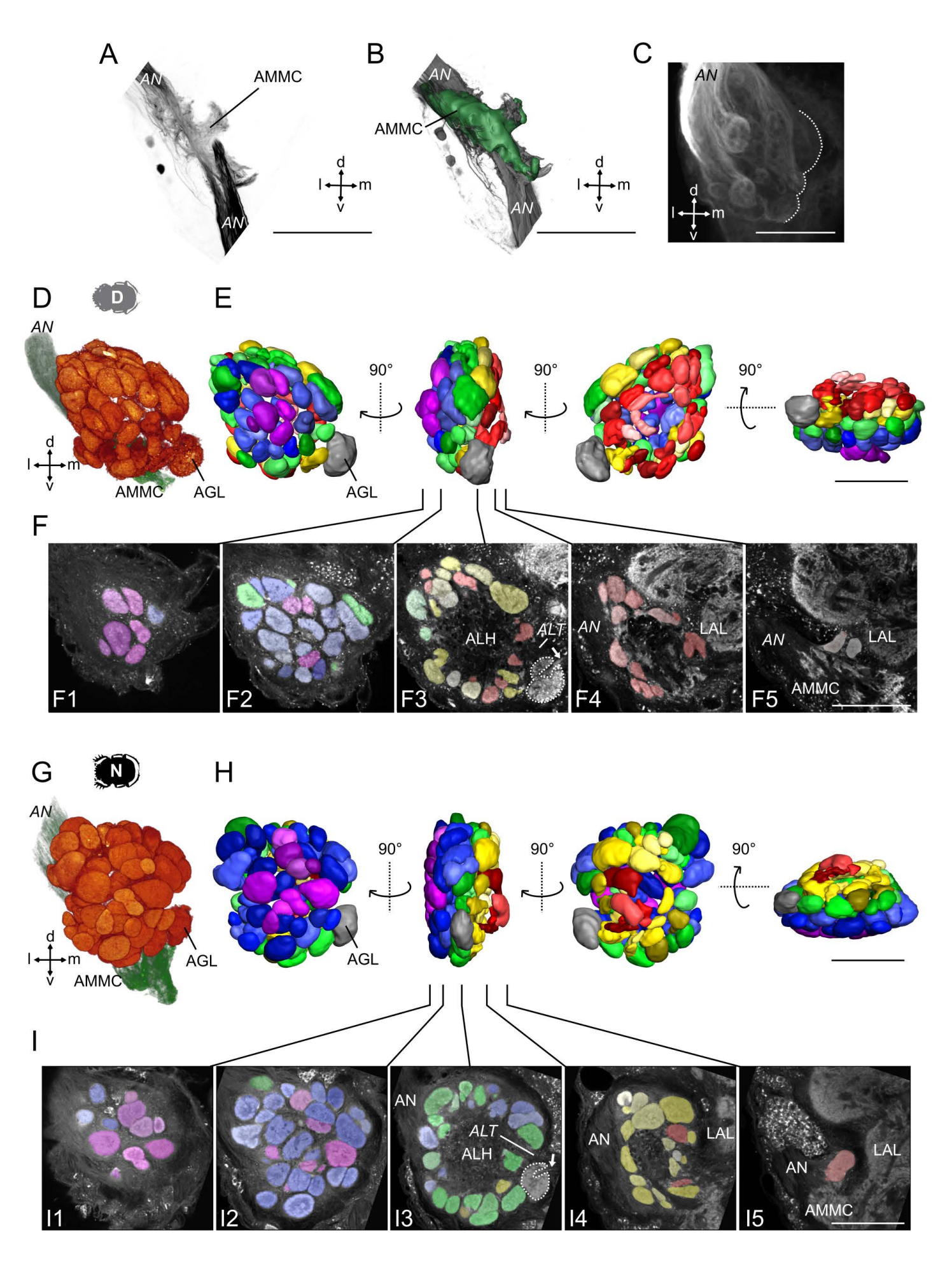
A
AN
AMMC
AN
d
l
m
v
B
AN
AMMC
AN
d
l
m
v
C
AN
d
l
m
v
D
D
AN
d
l
m
v
AMMC
AGL
E
90°
90°
90°
AGL
F
F1
F2
ALH
ALT
F3
AN
LAL
F4
AN
LAL
AMMC
F5
G
N
AN
d
l
m
v
AMMC
AGL
H
90°
90°
90°
AGL
I
I1
I2
AN
ALT
ALH
I3
AN
LAL
I4
AN
LAL
AMMC
I5

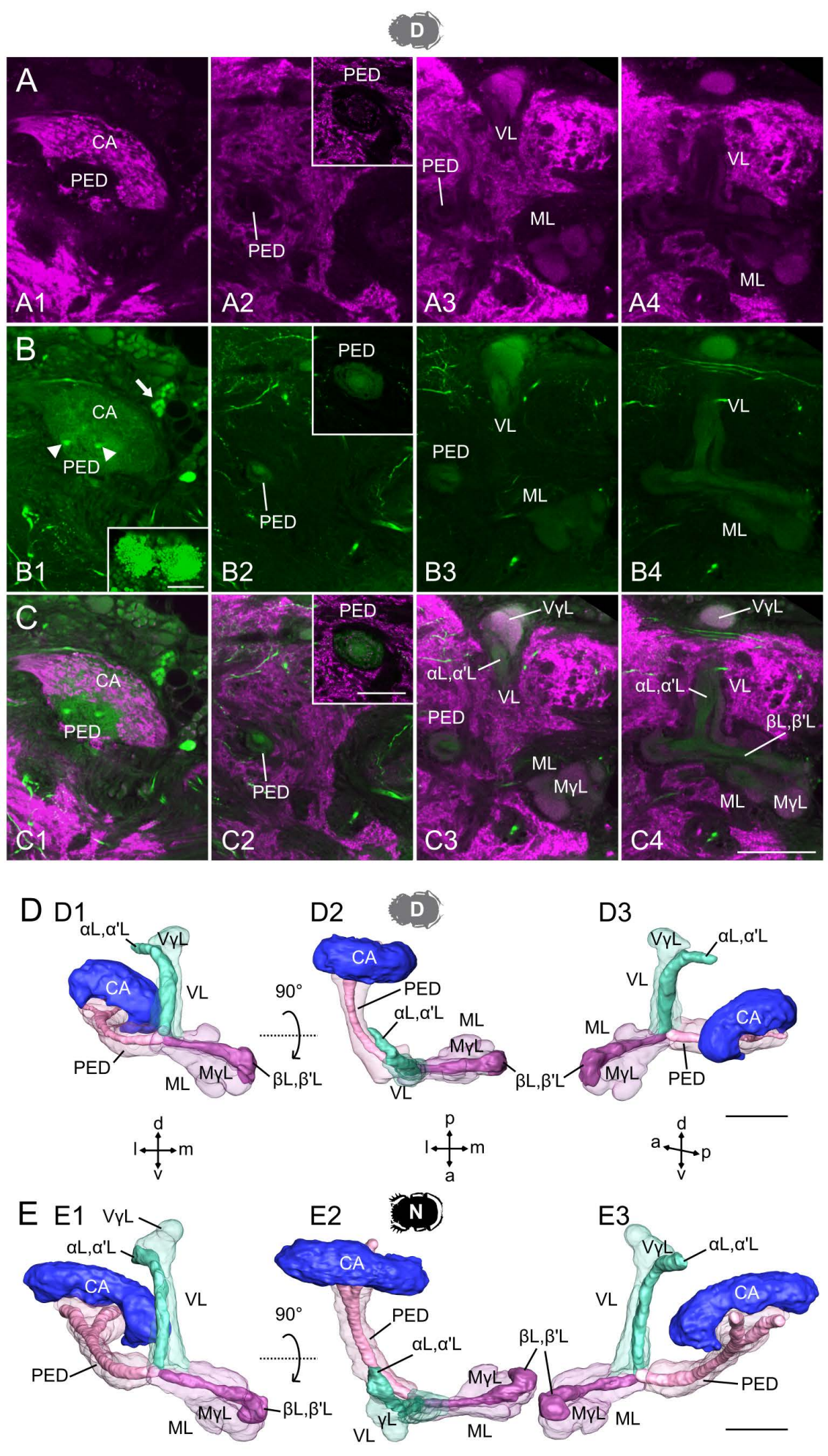
D
A
CA
PED
A1
PED
PED
A2
VL
PED
ML
A3
VL
ML
A4
B
CA
PED
B1
PED
PED
B2
VL
PED
ML
B3
VL
ML
B4
C
CA
PED
C1
PED
PED
C2
VγL
αL,α'L
VL
PED
ML
MγL
C3
VγL
αL,α'L
VL
βL,β'L
ML
MγL
C4
D
D1
αL,α'L
VγL
CA
VL
PED
ML
MγL
βL,β'L
90°
D2
D
CA
PED
αL,α'L
ML
MγL
βL,β'L
VL
D3
VγL
αL,α'L
VL
CA
ML
MγL
PED
d
l
m
v
p
l
m
a
d
a
p
v
E
E1
VγL
αL,α'L
CA
VL
PED
MγL
βL,β'L
ML
90°
E2
N
CA
PED
αL,α'L
βL,β'L
MγL
VL
ML
E3
VγL
αL,α'L
VL
CA
PED
MγL
ML

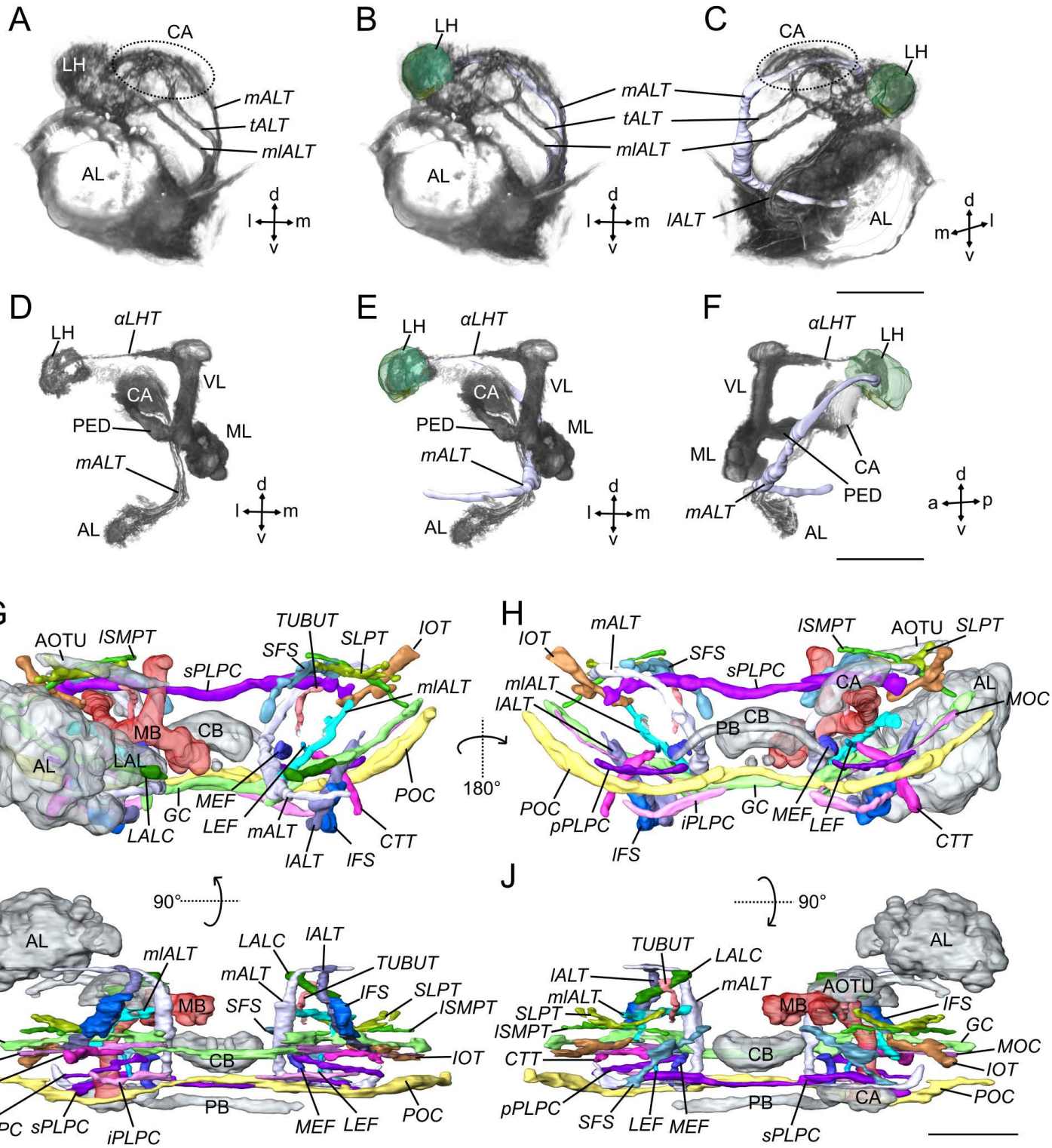
A
CA
LH
mALT
tALT
mlALT
AL
d
l
m
v
B
LH
mALT
tALT
mlALT
AL
C
CA
LH
lALT
AL
D
αLHT
LH
CA
VL
PED
ML
mALT
AL
E
αLHT
LH
CA
VL
PED
ML
mALT
AL
F
αLHT
LH
VL
ML
CA
PED
mALT
AL
a
p
G
AOTU
lSMPT
TUBUT
SLPT
IOT
SFS
sPLPC
mlALT
MB
CB
AL
LAL
GC
MEF
LEF
mALT
POC
LALC
lALT
lFS
CTT
180°
H
IOT
mALT
lSMPT
AOTU
SLPT
SFS
sPLPC
mlALT
lALT
CA
AL
MOC
CB
PB
POC
pPLPC
iPLPC
GC
MEF
LEF
lFS
CTT
I
90°
AL
mlALT
LALC
lALT
mALT
TUBUT
SFS
lFS
SLPT
lSMPT
MB
GC
MOC
CB
lOT
CTT
PB
pPLPC
sPLPC
iPLPC
MEF
LEF
POC
J
90°
AL
TUBUT
LALC
lALT
mALT
mlALT
AOTU
SLPT
MB
lFS
lSMPT
GC
CTT
CB
MOC
lOT
pPLPC
PB
CA
POC
SFS
LEF
MEF
sPLPC

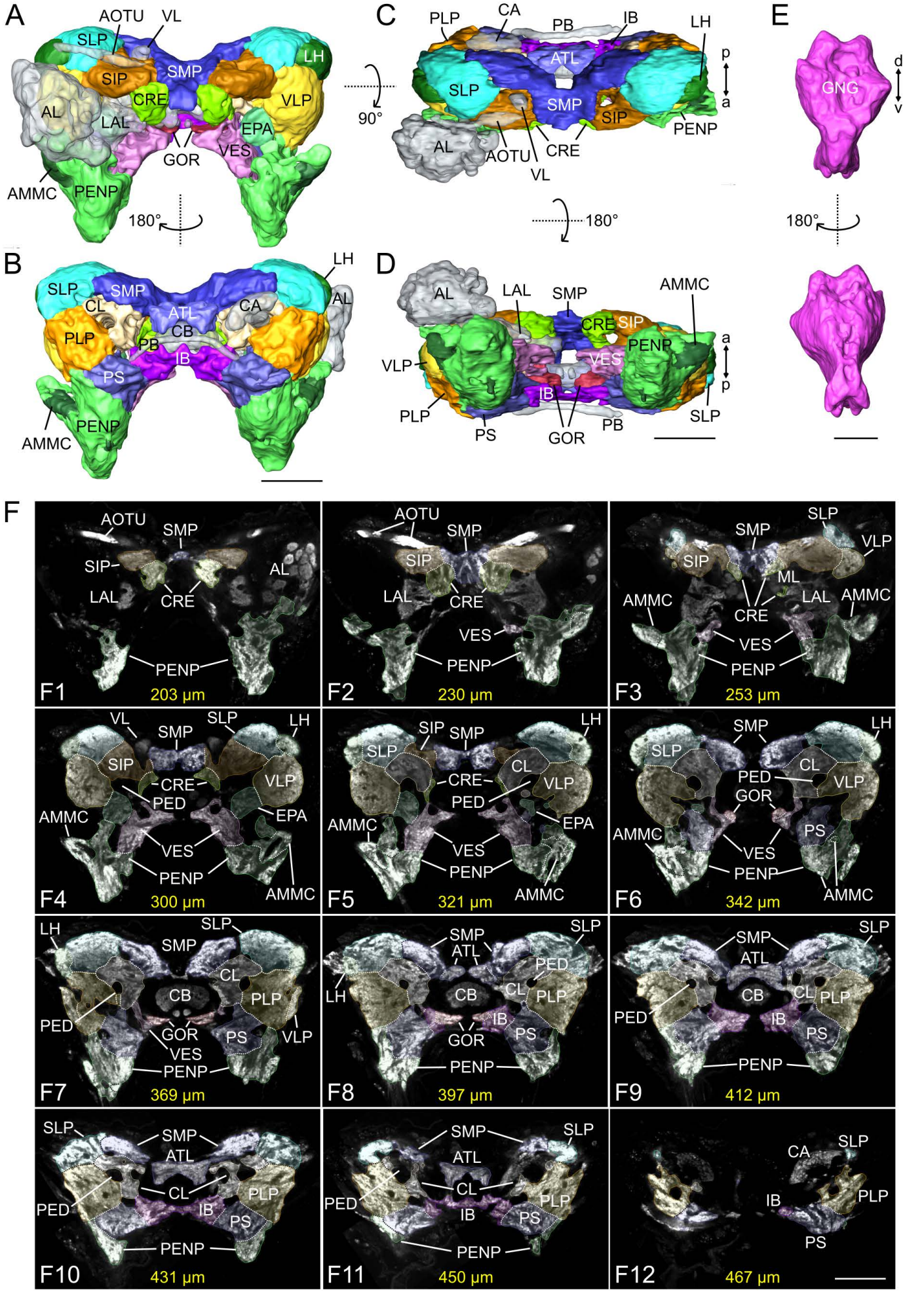
A
AOTU
VL
SLP
LH
SIP
SMP
CRE
VLP
AL
LAL
EPA
GOR
VES
AMMC
PENP
180°
B
LH
SLP
SMP
AL
CL
ATL
CA
CB
PLP
PB
IB
PS
PENP
AMMC
C
PLP
CA
PB
IB
LH
ATL
p
SLP
SMP
SIP
a
90°
PENP
AL
AOTU
CRE
VL
180°
D
AL
LAL
SMP
AMMC
CRE
SIP
a
PENP
VLP
VES
IB
p
PLP
PS
GOR
PB
SLP
E
GNG
d
v
180°
F
F1
AOTU
SMP
SIP
AL
LAL
CRE
PENP
203 µm
F2
AOTU
SMP
SIP
LAL
CRE
VES
PENP
230 µm
F3
SLP
SMP
VLP
SIP
ML
AMMC
LAL
AMMC
CRE
VES
PENP
253 µm
F4
VL
SMP
SLP
LH
SIP
CRE
VLP
PED
AMMC
EPA
VES
PENP
AMMC
300 µm
F5
SIP
SMP
LH
SLP
CRE
CL
VLP
PED
AMMC
EPA
VES
PENP
AMMC
321 µm
F6
SMP
LH
SLP
CL
PED
VLP
GOR
AMMC
PS
VES
PENP
AMMC
342 µm
F7
LH
SLP
SMP
CL
CB
PLP
PED
GOR
PS
VLP
VES
PENP
369 µm
F8
SMP
SLP
ATL
PED
LH
CB
CL
PLP
IB
GOR
PS
PENP
397 µm
F9
SMP
SLP
ATL
PED
CB
CL
PLP
IB
PS
PENP
412 µm
F10
SLP
SMP
ATL
CL
PED
PLP
IB
PS
PENP
431 µm
F11
SMP
SLP
ATL
CL
PED
PLP
IB
PS
PENP
450 µm
F12
CA
SLP
IB
PLP
PS
467 µm

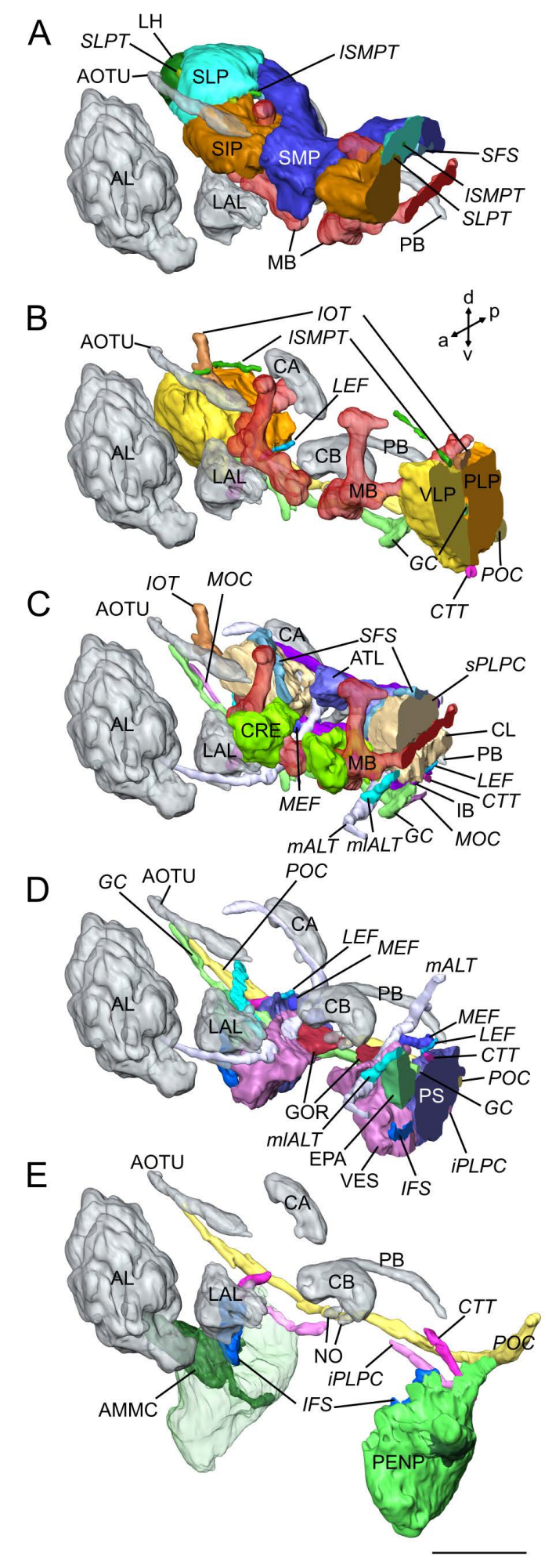
A
LH
SLPT
AOTU
SLP
ISMPT
SIP
SMP
SFS
AL
LAL
ISMPT
SLPT
PB
MB
B
IOT
AOTU
ISMPT
d
p
a
v
CA
LEF
AL
CB
PB
LAL
MB
VLP
PLP
GC
POC
CTT
C
IOT
MOC
AOTU
CA
SFS
ATL
sPLPC
AL
CRE
CL
LAL
PB
MB
LEF
MEF
CTT
IB
mALT
mlALT
GC
MOC
D
GC
AOTU
POC
CA
LEF
MEF
mALT
AL
PB
CB
LAL
MEF
LEF
CTT
POC
PS
GOR
GC
mlALT
EPA
VES
IFS
iPLPC
E
AOTU
CA
PB
AL
CB
LAL
CTT
NO
POC
iPLPC
AMMC
IFS
PENP